Design and Development of Shape memory alloy based E-glass resin composite structure its applications for a missile fin

Masters of Technology Thesis

By

Pydi Yeswanth Sai

(mt1602181005)

Under the Guidance of

Dr.I.A.Palani

Dr. Amod C. Umarikar

DISCIPLINE OF METALLURGY ENGINEERING AND MATERIAL SCIENCE

INDIAN INSTITUTE OF TECHNOLOGY INDORE

INDIAN INSTITUTE OF TECHNOLOGY INDORE

CANDIDATE'S DECLARATION

I hereby certify that the work which is being presented in the thesis entitled Design and Development of Shape memory alloy based E-glass resin composite structure its applications for a missile fin in the partial fulfillment of the requirements for the award of the degree of **MASTER OF TECHNOLOGY** and submitted in the **DISCIPLINE OF Metallurgy and Material science, Indian Institute of Technology Indore**, is an authentic record of my own work carried out during the time period from july 2017 to july 2018 under the supervision of Dr. I.A. Palani, HOD, associate professor and Dr. Amod C. Umarikar, Associate Professor

The matter presented in this thesis has not been submitted by me for the award of any other degree of this or any other institute.

Signature of the student with date

Pydi Yeswanth Sai

This is to certify that the above statement made by the candidate is correct to the best of my/our knowledge.

Signature of the Supervisor of M.Tech. thesis #1	Signature of the Supervisor of M.Tech. thesis #2
Dr. I.A. Palani	Dr. Amod C. Umarikar,

Pydi Yeswanth Sai has successfully given his/her M.Tech. Oral Examination held on **4th July 2018**.

Signature(s) of Supervisor(s) of M.Tech. thesis

Convener, DPGC

Date:	Date:
Signature of PSPC Member #1	Signature of PSPC Member #2

ACKNOWLEDGEMENT

I would like to express my sincere gratitude to my research guides **Dr. I.A.Palani**, and **Dr. Amod C. Umarikar** for their constant encouragement, guidance, and support from the preliminary stage to the concluding level of research work.

I express my sincere thanks to Pushpendra singh, DRDO Research Center Imarat, Hyderabad for providing me an opportunity to carry out the project with his constant support and suggestions throughout my research work.

I wish to thank my PSPC members Dr. Indrasen singh and Dr. Eswara Prasad Korimilli for their valuable suggestions right from the beginning of my work.

I personally thank Dr. Subbareddy Daggumati for his technical support in understanding composite materials and their fabrication techniques.

I also express my sincere gratitude to Sophisticated instrumentation center (SIC), for providing me the necessary characterization facility throughout my research work.

I would like to thank each and every faculty member in the department of Metallurgy and Material science for their technical support at various stages right beginning from the course work

I would like to thank my colleagues in Mechatronics and instrumentation Laboratory Mr Mani Prabhu S S, Mr. Akash, Mr Tameshwar Nath Tiwari, Mr Ashish Shukla, Ms Nandini patra, Mr Jayachandran, Mr Rajagopalan, Ms Ankitha Sahu, Mr Abhinav Sharma, Mr Akhil verma, Mr Anandh kumar and Mr Suhel Khan for their suggestions and timely solutions for the problems encounterd during the research work. My sincer thanks to Mr. Sachin bhirodkar, Lab manager for sorting out the official issues on right time.

I extend my cordial thanks to all the staff members of SIC, Central workshop, Central Library, Academic Section, Accounts section of IIT Indore for their kind cooperation.

Last but not least, I am eternally grateful to my father P Venkata Ramana and to my Mother P Padmavathi for the acknowledge affection, support and moral encouragement which has been provided throughout my carrier.

LIST OF PUBLICATIONS

International Conferences

- **Yeswanth Sai**, Suhel Khan, Mani Prabu S S, Palani I A, Amod C Umarikar, Pushpendra Singh Development, Actuation and Material Analysis of Shape Memory Alloy Reinforced Composite Flapper, conducted by International conference on Composite materials(ICCMMEMS-2018)

- **Yeswanth Sai**, Suhel Khan, Mani Prabu S S, Palani I A, Amod C Umarikar, Pushpendra Singh Active Control of Shape Memory Alloy Composite Flapper for aerodynamic applications, conducted by International conference on Robotics, Smart structures (RoSMA-2018)

- Jayachandran S, Akash K, Mani Prabu S. S, Shraddha Rahul D, **Yeswanth Sai**, Palani I A Realization of Actuation Characteristics of as fabricated NiTi Bimorph for MEMS device development

Chapter 1 Shape memory alloy based composite structures

Chapter 2 Fabrication of Smart structure

Chapter 3 Thermo-mechanical actuation of smart structure .

Chapter 4 Crystallization effect on the actuation of the smart structure

Chapter 5 Variation in the surface temperature and stress distribution on the smart structure due to air flow

List of figures

List of tables

Chapter 1 Shape memory alloy based composite structures

1.1. Introduction

From centuries conventional metals have played a significant role as structural materials. With advancement in science and technology these materials can no longer fulfil the requirements, hence a new class of multi-functional materials (Smart materials) have emerged. Smart materials incorporated with a structural material, together can be termed as SMART STRUCTURE. Smart structure’s and their control is the field of scientific endeavor, which includes the study of material science and various engineering fields like controllers, actuators, and sensors. This study in-turn helps to understand and generate the fundamental principles of material actuation and its coherence with sensors and controllers. SMA based composite structure is sort of smart structures where the thermo-mechanical behaviour of SMAs are used for actuation and elastic rigidity of E-glass composite structure used for retentation to its initial position

Shape memory alloys are the class of smart materials, whose ability is to recover their initial shape at a certain elevated temperature or to withstand large strains without plastic deformation or failure. The former one is called as shape memory effect and the later one is termed as super-elasticity [1,2]. In order to recover its initial shape SMAs are undergoes diffusion less phase transformation i.e from high temperature symmetric, austenitic phase to low temperature asymmentric, martensitic phase

“A Composite material is defined as a material which is composed of two or more materials at the microscopic level and has chemically distinct phases”. Thus, the composite material is heterogeneous at a microscopic scale but statically homogeneous at the macroscopic scale. Composites defined in this thesis are manufactured from fibers mixed with a (polymer) resin or matrix. E-glass based unidirectional fibers are chosen because of its high elastic module and tensile strength over woven fibers. Bisphenol-A based epoxy resin was used as a resin (polymer) in order to bind the fibers together.

Currently, most of the structural materials have been replaced with epoxy based composite structures, since there are cost effective, possess the high strength to density ratio, design flexibility, and highly corrosive resistant. NiTi SMA’s are chosen because of their high actuation energy and high volumetric output, whereas unidirectional fibers have been chosen because of their high elastic module compared to woven fibers.

In fabrication of Ni-Ti based smart structures equi-atomic NiTi SMA wires are used as a smart materials and unidirectional glass fiber reinforced composite structure is used as the structural material. Thermo-mechanical behavior and the material properties of the structure before and actuation were analyzed. A novel approach of studying the material properties before and after actuation of the smart structure and its influence on the failure of the structure was analyzed. The developed smart structure displayed shape memory effect without training of SMA. Investigations on the experimental parameters like volume fraction of SMA, the rate of straining and multi cycle behavior of SMA have been investigated. In order to analyze the material properties XRD, DSC and SEM were performed.

1.2 Actuation Mechanism of SMA and SMA based smart structures

In order to understand the actuation mechanism of SMA based smart structure, it is necessary to have a prior understanding of shape memory alloy actuation.

In this thesis my primary consideration about shape memory effect (SME), which is actually a thermo-mechanical based actuation. Shape memory alloy undergoes a metallurgical phase transformation from twinned martensite to de-twinned martensite on the application of external loads. The martensitic phase will have different crystal phases like (tetragonal, orthorhombic and monoclinic) whereas austenite phase will have a cubic crystal structure in general. In absence of external load, the structure from de-twinned martensite changes into austenite phase under application of thermal loads. This phase transformation from one structure to another happens due to shear lattice deformation but not due to diffusion of atoms. This kind of transformation is known as martensitic transformations.

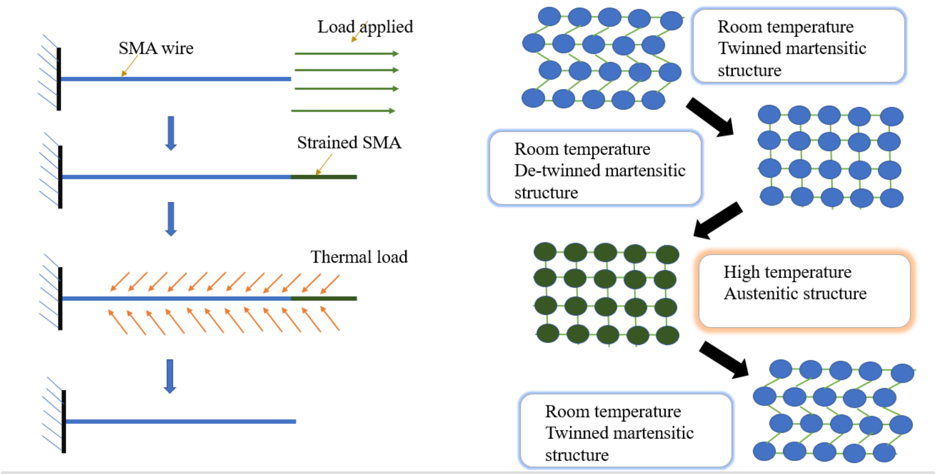

Figure 1.1 Schematic of SMA wire, phase transformation with reference to its crystal structure

Above schematic is for one-way shape memory effect, where for each and every cycle of actuation there should be a bias load in order to transform twinned martensitic structure to de-twinned martensitic structure. In SMA based composite structure the necessity of bias load was eliminated with the help of structural property (elastic rigidity) of GFRP. Pre-strained NiTi SMA wires are embedded into the layers of GFRP and cured under atmospheric conditions. Thus, for each and every actuation SMA will convert from austenite to de-twinned martensitic structure with its initial strain condition without application of any bias load.

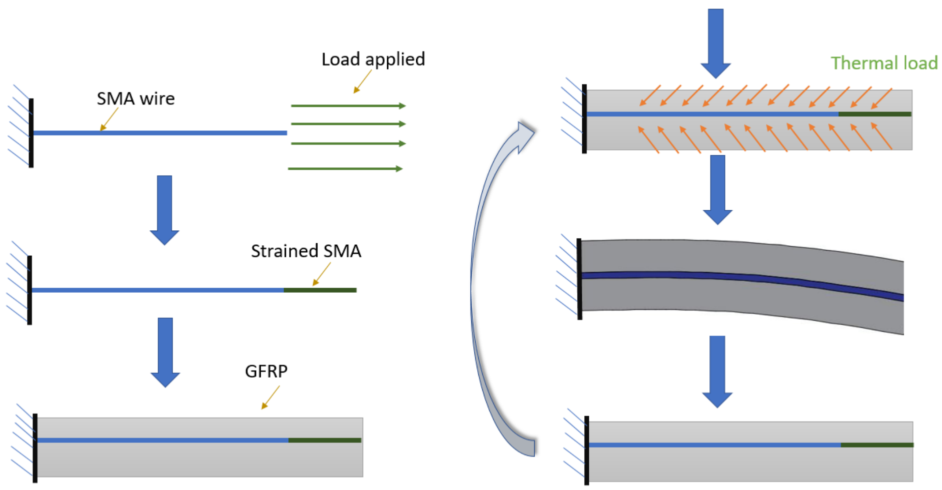

Figure 1.2 Schematic representation of SMA GFRP actuation mechanism

1.3 Literature survey

Many researchers have studied the thermo-mechanical actuation models for the deformation of SMA composites M Moallem [3] et.al studied the "Deflection control of a flexible beam using shape memory alloy actuators" where he develops a nonlinear control scheme for deflection control of a flexible beam system using shape memory alloy (SMA) smart actuators. A J Z˙ ak [4] et.al studied the "One-dimensional shape memory alloy models for use with reinforced composite structures" where he developed a various model that are attributed to Tanaka, Liang and Rogers extensively in the literature for studying the static or dynamic performance of different composite material structures with embedded shape memory alloy components. Saptarshi Karmakar [5]et.al studied the "Optimum placement of shape memory alloy wire actuator" where he studies the effects of offset distance, and the number of points called attachments, where the shape memory alloy wire is connected to a host beam. Gangbing Song [6] et.al studied the "Active position control of a shape memory alloy wire actuated composite beam" where he designed and experimented for the active control of the shape memory alloy composite structure using joule heating setup.

Thermo-mechanical actuation of the composite structure by using pre-strained SMA wires are widely explored but there are a few who have tried it by training of SMA. A. Fortini et.al [7–13]studied different aspects of SMA applications, significantly on"TWSME of a NiTi strip in free bending conditions: experimental and theoretical approach" where he trained an equi atomic NiTi to shape memory alloy and studied its deformation. Theoretical analysis on the life of trained SMA was studied but an experimental study was missing. Hugo Rodrigue[14] et.al studied the "Cross-Shaped Twisting Structure Using SMA-Based Smart Soft Composite" where he develops a SMA composite structure which can produce a twisting moment in the structure when it is thermo-mechanically actuated.

SMA composites developed are utilized in many applications. Many researchers have studied the applications of SMA composites developed, Annalisa Fortini et.al studied the "Morphing blades with embedded SMA strips: An experimental investigation" where he experimentally developed a composite blade for an automotive axial fan. Min-Woo Han [15] et.al studied the “Woven type smart soft composite for soft morphing car spoiler” where he develops a SMA composite structure which can be used as a car spoiler. Hyung-Jung Kim[16] et.al studied the “A turtle-like swimming robot using a smart soft composite (SSC) structure” where he develops a SMA soft composite structure for under water applications. Wei Wang [17] et.al studied the “Locomotion of inchworm-inspired robot made of smart soft composite” where the SMA based soft composite structure moves linearly and angularly, which resembles an inch worm movement.

Although many types of research have studied the thermo-mechanical actuation, theoretical simulation on SMA placement and its straining effects during actuation, applications of SMA composites in various mechanical and biological objects are quite elaborately explored. However, reports on significant topics such as relaibility and failure analysis of the smart srtuctures are less. Post material analysis on the GFRP structure after thermo-mechanical actuation are quite rare. In the current study change in the material properties of GFRP and its impact on the life of the SMA composite structure after thermo-mechanical actuation was analyzed.

1.4 Motivation and Objective

A smart structure fabricated by SMA and GFRP has a lot of engineering applications and few of them are listed in section 1.3. Although the smart structure has a wide range of applications it was limited to few of them in general. Repeatability and reliability of the smart structure were one of the major issues that needed to be addressed. Thermo-mechanical actuation of the smart structure was limited to few cycles. From figure 1.3 it is clear that the SMA actuates 3.5mm 0.12million cycles whereas the smart structure fabricated actuates only for 7 complete cycles. Hence the cause for the failure of multi cycle actuation for a smart structure are to be addressed.

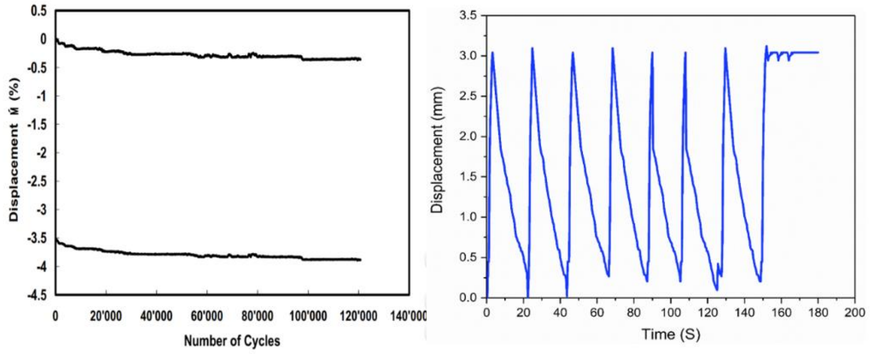

Figure 1.3 Multicycle actuation of SMA wire and Smart structure

The thesis outline stands derived from the primary objectives, and the chapter’s outline is given below

Chapter 1: Introduction to Shape memory alloys, epoxy based composites and the smart structures.

Chapter 2: Fabrication of SMA composite structures.

Chapter 3: Thermo-mechanical actuation of the smart structure.

Chapter 4: Epoxy-crystallization effect on the failure of the Smart structure.

Chapter 5: Variation in the surface temperature and stress distribution on the smart structure due to air flow

Chapter 6: Conclusion obtained from the experimental investigations and the scope for future work.

Chapter 2 Fabrication of Smart structure

Fabrication of SMA based smart structure has been divided into two parts. In the first part, we will see how the SMA wires have been stained and in the later phase, we will discuss the composite structure fabrication with SMA.

2.1 Materials required

The SMA wires chosen for the current study were equal-atomic NiTi alloy wire, with 0.5mm diameter. The structural material is made up of uni-directional E-glass fibers and the resin (polymer) is made up of Bisphenol-A with a suitable hardener for vinyl polymers. Glass fiber of 0.36mm with 1200tex are chosen, to achieve moderate strength and stiffness for the composite fabricated. Both fiber and resin were procured from the Hindoosthan composites solutions, Mumbai, India. Epoxy resin and the hardener are mixed in the ratio of 100:30, which is prescribed by the manufacture

2.2 Straining of SMA wires

To convert the twinned martensitic structure of SMA to de-twinned, the SMA's are subjected to strain under tensile loading conditions. In order to strain SMA's, a 100N load computerized straining gauge manufactured by the Fine manufacturing industries, pune, India was used. SMA wires are clamped to a specially designed wire holder chucks, and a constant head speed of 2mm/min was maintained while the wire was subjected to straining. SMA wires are strained to 5%, 4%, 3% and 2% before they embedded in the GFRP.

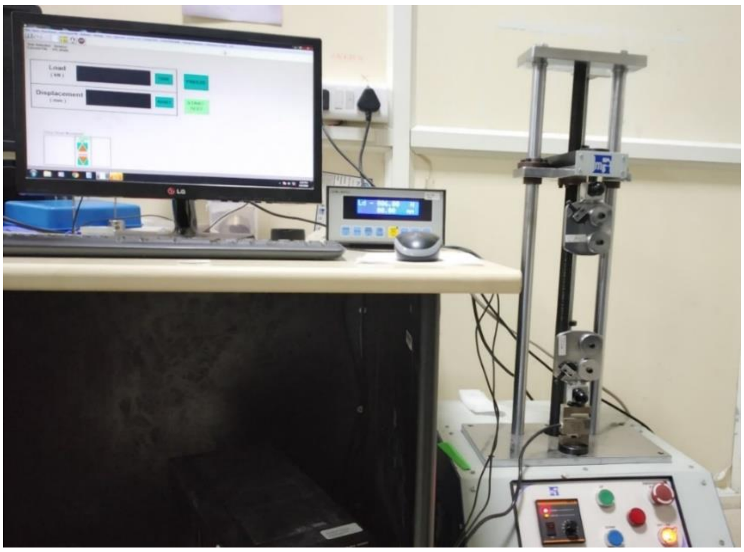

Figure 2.1 Straining gauge setup for SMA wires

2.3 Vacuum assisted resin transfer moulding

Smart structures are fabricated by using vacuum assisted resin transfer moulding (VARTM) or simply vacuum bagging method. In this method of fabrication, SMA wires are stacked in between the layers of glass fiber and entire stacking will be sealed inside the mould box. Two inlets will be provided at two extreme ends of the mould. To one end, vacuum pump inlet was connected and to the other end, inlet pipe of epoxy resin will be connected. When the vacuum was created inside the mould, due to pressure difference resin will start flow from one end to the other end of the mould. Precaution to be taken such that epoxy resin should not enter the vacuum pump.

Table 2-1 Equipment's and their use in VARTM process

Equipment	Purpose
1. Vacuum pump	To create vacuum
2. Vacuum bagging film	Air tight seal placed over the sealant tape.
3. Breather and bleeder	Traps and holds excess resin from laminate
4. Release peel ply	Provides an easy release of the laminate structure after curing
5. Release film	Optional* Applied on mould surface for easy removal of laminate
6. Flow pipes with two way shut off valves	Maintain a controlled flow of epoxy resin
7. Mould surface	Replica of the final laminate composite structure
8. Sealant tape	Seals the bag to the mould
9. Glass jar	To avoid the flow of epoxy into the vacuum pump

Once the epoxy resin got in penetrated into the fibers, we will shut off the valves and allow the setup undisturbed for 24hrs under atmospheric conditions. The vacuum developed inside the mould ensures uniform flow of resin throughout the structure. After 24 hours' epoxy resin will get cured and the developed GFRP act as a smart structure.

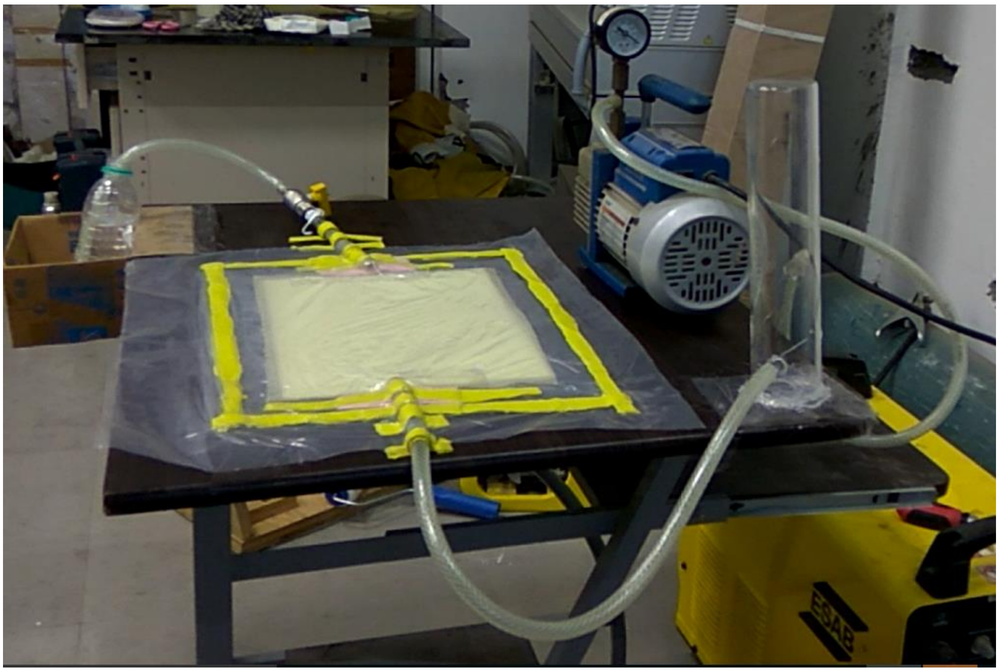

Figure 2.2 VARTM setup for smart structure fabrication

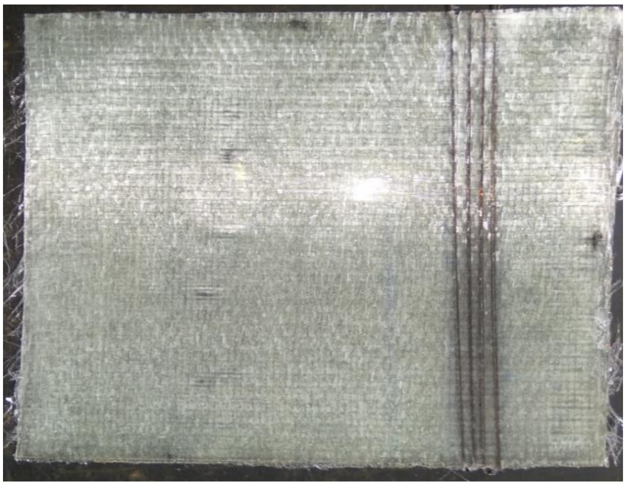

Figure 2.3 Smart structure fabricated by using VARTM method

2.5 Experimental setup to actuate the Smart structure

SMA based smart structures are actuated via joule heating. Thermo-mechanical actuation of smart structure needs to follow a standard experimental procedure. The experimental setup consists of smart structure, a programmable power supply for supplying electricity, an infrared laser sensor to detect the beam tips displacement (LDS), real-time data acquisition (DAQ) system and PID controller.

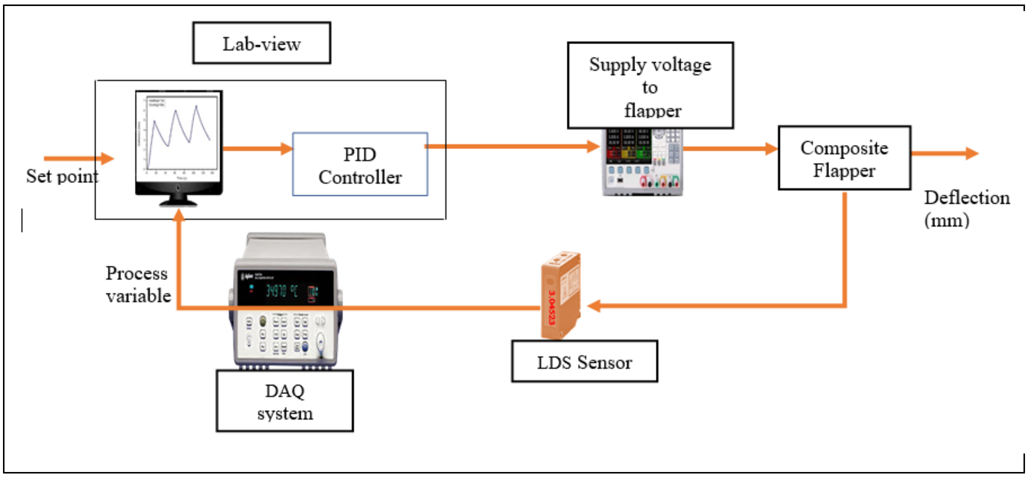

Figure 2.4 Experimental setup for thermo-mechanical actuation of smart structure

LDS is a noncontact type displacement sensor which measures the deflection of the smart structure. DAQ collects the data from the LDS and its process to the interfaced PC. PID controller was used for active control of the smart structure, where the supply will get a turn of if the smart structure actuates beyond its threshold value.

Current works carry the preliminary research to optimize the actuation parameters of the smart structure and its reliability for multi-cycle actuation. Hence work on active control of smart structure was not explained in detail and the complete thermo-mechanical actuation work was carried out in passive control. Due to the absence of PID controller, the power supply will be controlled manually.

Chapter 3 Thermo-mechanical actuation of smart structure

3.1 Mechanism of Thermo-mechanical actuation

Placement of SMA wires in the fabrication of smart structures plays an important role. While fabrication, SMA wires are placed eccentrically from the neutral plane of the composite structure. As mentioned earlier, joule heating will try to retrain the strains induced in SMA before fabrication of the smart structure. Since SMA's are placed eccentrically from the longitudinal axis of the structure, the retrieving forces developed in SMA's will in-turn generate a reaction forces (in equal and opposite direction) in the composite structure to attain static equilibrium conditions. Hence a couple force generates in the composite structure, deflects the Smart structure.

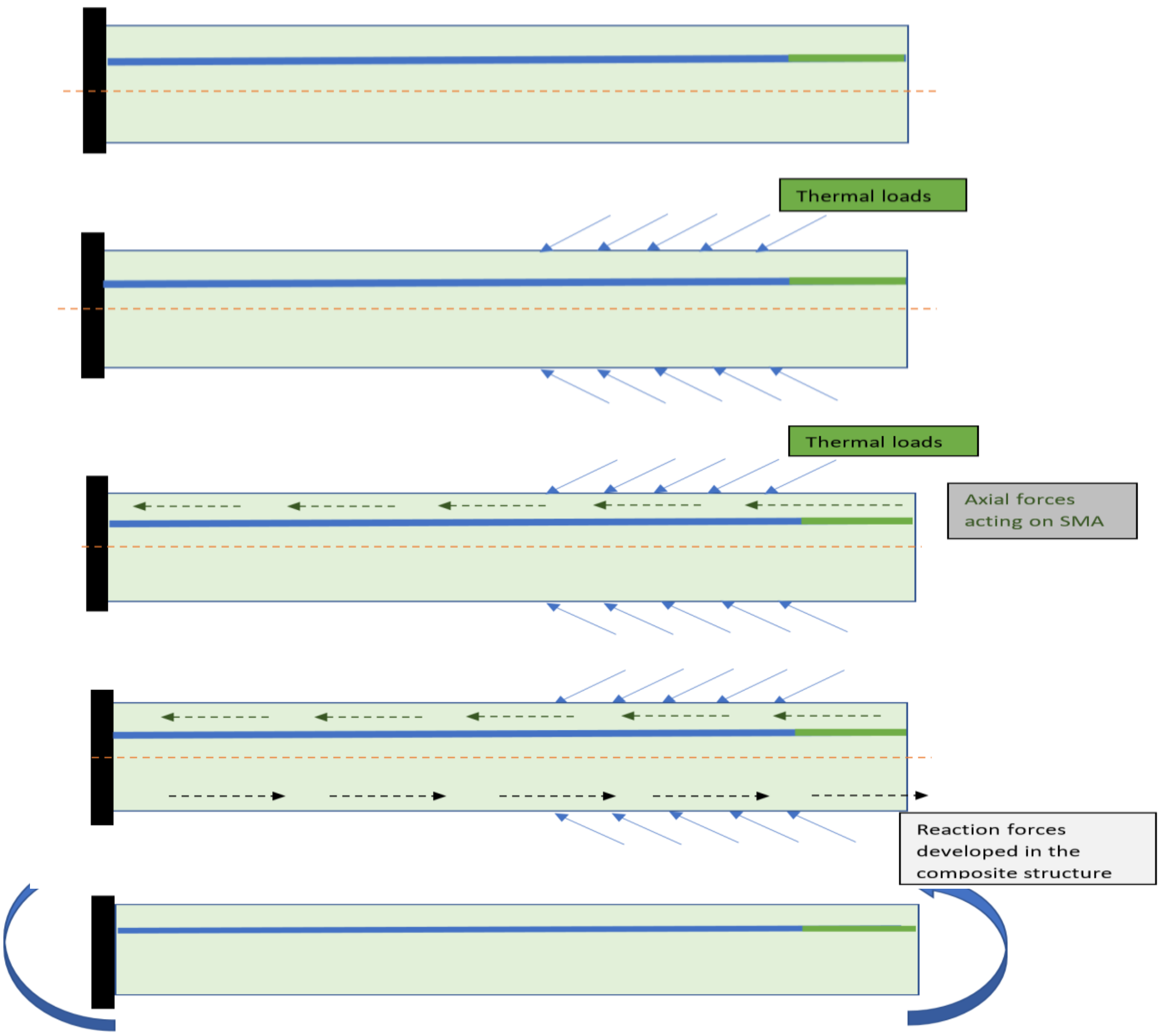

Figure 3.1 Mechanism of thermo-mechanical

.

A smart structure fabricated by VARTM method can be seen in figure 3.2. The fabricated smart structure was then machined into a rectangular beam with dimensions of 250*25*5 mm. GFRP structures without SMA are used in tensile test, to determine the strength and modulus of the GFRP.

Figure 3.2 Smart structure machined from a GFRP plate

a

b

c

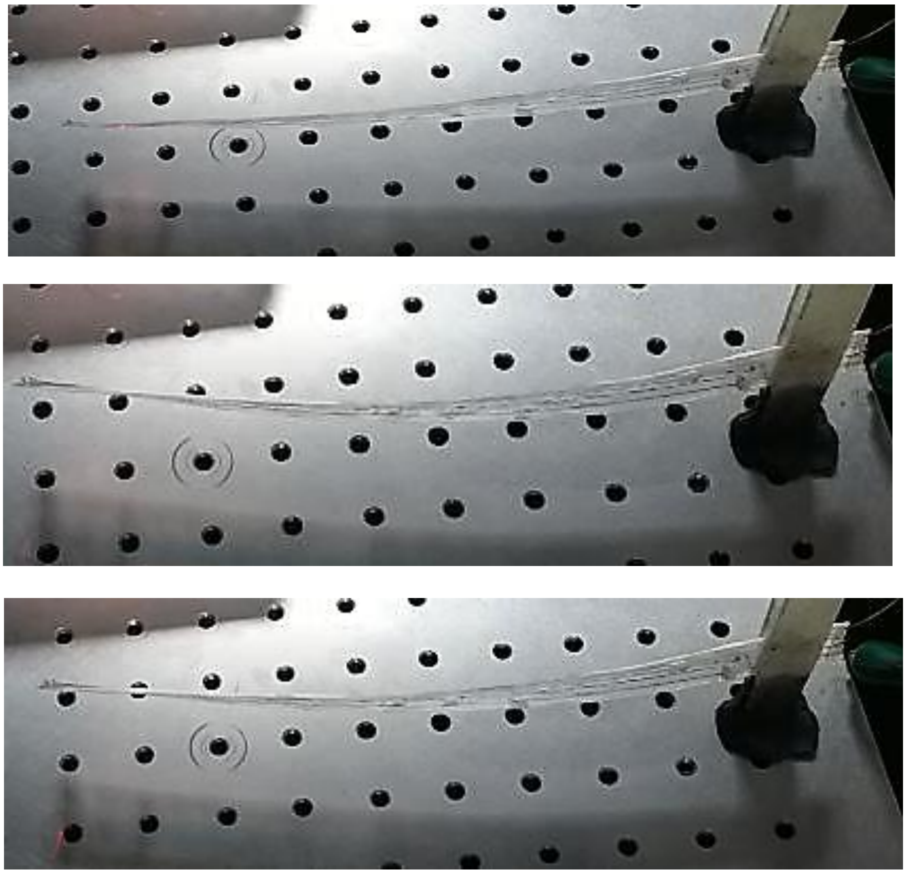

Figure 3.3 Actuation of a smart structure via joule heating setup

Smart structured beam actuated via joule heating can be seen in figure 3.3. In this entire work, in order to perform thermo-mechanical actuation parameters such as current and voltage were fixed. To perform actuation, a constant current of 2A and voltage of 10V was supplied through the thermo-mechanical actuation. Smart structure was joule heated for 5 seconds and subsequently cooled for 15 seconds. Figure 3.3a was the initial position of the smart structure. When we supplied power, the smart structure will get actuated and it can be seen from figure 3.3b and 3.3c.

Thermo-mechanical actuation of the smart structure involves certain processing parameters which should be optimized. Processing parameters like material properties of SMA, fiber configuration of the composite, volume fraction of SMA in a composite structure, percentage of SMA strained, length of the smart structure etc. To optimize each and every parameter experimentally is too tedious and cost effective. Hence parameters like material properties of SMA and fiber configuration are optimized through literature and other processing parameters are optimized experimentally.

W.Huang[18] et.al experimentally determined the actuation parameters of CuAlNi, NiTi, CuZnAl. By considering these parameters, we have chosen NiTi for this work.

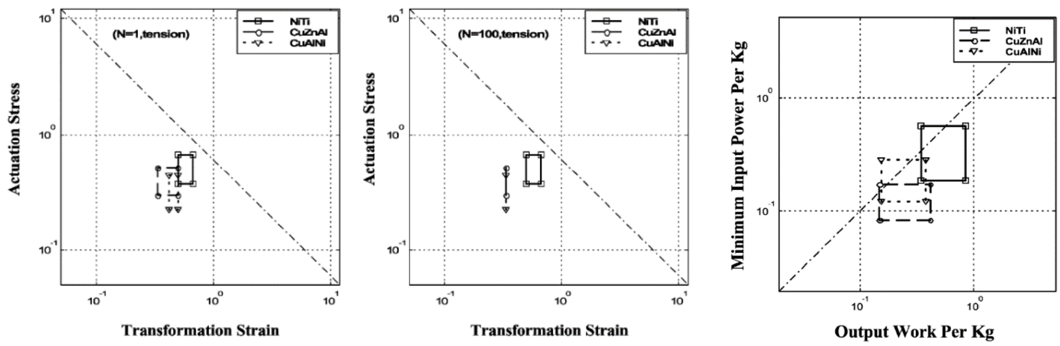

Figure 3.4 Comparison of actuation characteristics of CuAlNi, NiTi, CuZnAl

From the figure 3.4, it is clearly evident that NiTi produces more actuation stress and output work compared to CuAlNi and CuZnAl.

S. Eksi and K. Genel [19] et.al studied the mechanical properties of unidirectional and woven fibres of both glass and carbon. They experimentally determined the mechanical properties of all the composite fibres by conducting tensile, compressive and shear tests.

By considering these properties, E-glass unidirectional fibers are having high strength and elastic modulus compared to woven fibers. Although carbon and aramid fibers are having higher strength and modulus, but there are not cost effective. Hence I adopted E-glass unidirectional composite fibers throughout my work.

Reinforcement type	Volume of fiber V_f	Density [g/cm^3]	Elasticity module [MPa]	Shear module [MPa]	Poison ratio [-]	Tensile strength [MPa]	Tensile strength/ density	Shear strength [MPa]	Compression strength [MPa]	Elongation at break
Woven glass	30	1.55	14 352	4728	0.24	220	141.9	119	96	0.016
Woven aramid	30	1.2	19 087	2585	0.38	357	297.5	53	64	0.019
Woven carbon	30	1.31	42 000	12350	0.32	340	259.5	180	118	0.009
Unidir. glass (0°)	30	1.55	18 300	3895	0.25	432	278.7	30	71	0.028
Unidir. glass (90°)	30	1.55	7 940	3895	0.17	52	33.5	30	16	0.0096
Unidir. carbon (0°)	30	1.31	78 715	2195	0.4	826	630.5	20	118	0.0100
Unidir. carbon (90°)	30	1.31	4 930	2195	0.25	37	28.2	20	27	0.0130

Figure 3.5 Mechanical properties of fiber reinforced composite structures

By considering the above mentioned properties of both SMA and composite fibers, I concluded NiTi SMA and E-glass unidirectional fibers for my entire work.

3.2 Optimization of SMA volume fraction in smart structure

To optimize the other properties like volume fraction of SMA in a composite structure, percentage of SMA strained, length of the smart structure, an experimental analysis has been conducted and those properties are optimized.

Volume fraction (V_f) of SMA in a composite determines the total volume of SMA present in the total volume of the composite structure. V_f of SMA actually defines the rate of actuation of the structure. From fig 3.6 its clearly evident that when V_f changes from 4% to 6% there was a drastic increase in the range of actuation.

Above mentioned we joule heated the smart structure for 5 seconds and cooled up to 15 seconds. Although the range of actuation was increased there was a slight deviation from the rate of actuation and it prolongs as we increase the cycle range. It's interesting to analyze the rate of actuation when V_f has been increased from 6% to 8%. Since increment in V_f causes a drastic increase in the range of actuation when it is at 6%, whereas at 8% of V_f not only the rate of actuation was increased but a permanent deformation was observed. The increment in V_f not only increases the range of actuation but also increases the temperature of the smart structure, hence the rigidity of the structure was lost and it cannot regain it back in 15 seconds of cooling

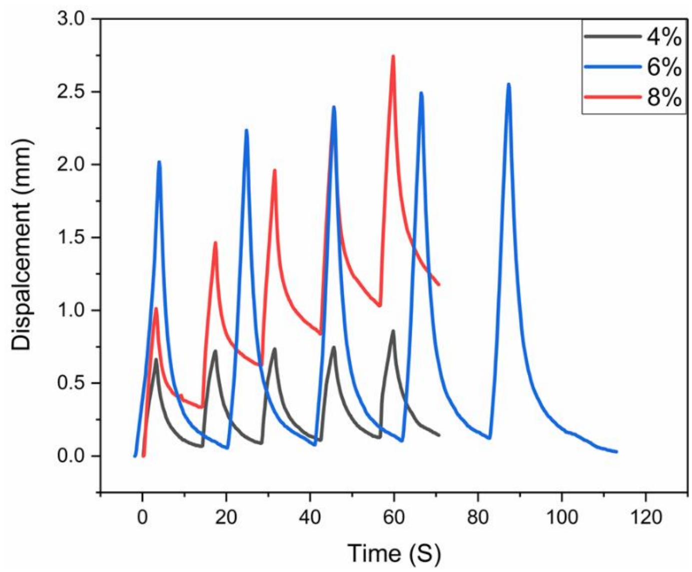

Figure 3.6 Thermo-mechanical actuation of the smart structure by varying volume fraction of SMA

Hence as the actuation cycles proceed further, there deformation in the structure also increases.

From the above results in figure 11, it can be concluded that 6% of V_f was optimal, and all further experiments are carried out by maintaining 6% of V_f as a constant parameter

3.3 Optimization of SMA straining in the smart structure

One of the important parameters in thermo-mechanical actuation of the smart structure was straining. Since straining of SMA wires will cause them to transform from twinned martensitie phase to de-twinned martensitic phase. Optimizing the level of strain will further optimize the actuation range of the smart structure.

Smart structures with the different strain levels are fabricated and their actuation characteristics are examined. SMAs are strained to 3%, 4%, 5% and the smart structure are maintained with 6% of SMA V_f. From figure 3.7 it is clearly evident that the structure with the higher amount of strain actuates to a higher range compared to 4% and 3%.

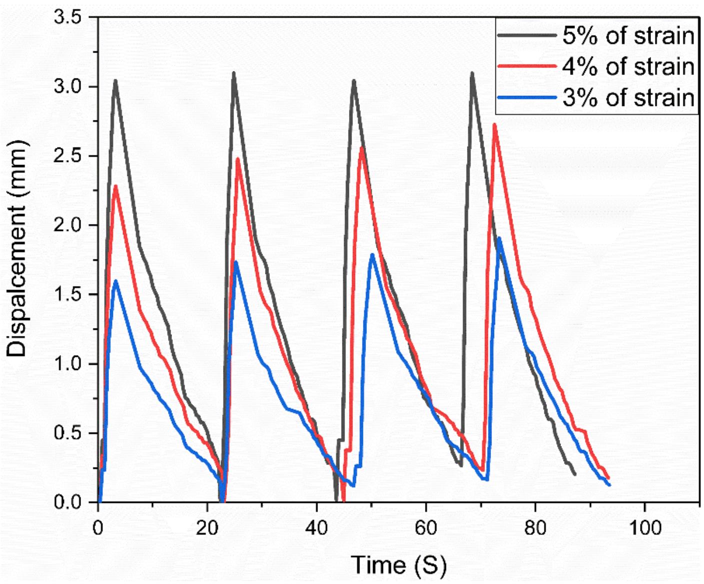

Figure 3.7 Thermo-mechanical actuation of the smart structure by varying volume fraction of SMA

Niti wires can be strained to a maximum level of 8%. NiTi strained beyond 8%, will not retrieve back the induced strain and it leads to permanent deformation in the structure. Considering the FOS, SMA's are strained up to 5%. Further experimental works are carried by keeping 6% of V_f and 5% strain level as constant processing parameters.

3.4 Optimizing the length of the smart structure

Actuation mechanism of the smart structure was explained in detail at the beginning of chapter 3. The bending moment developed inside the smart structure because of eccentric placement of SMA from the neutral axis. As the position of the SMA wires from neutral axis was increased the actuation range of SMA was also increased, but while actuation SMA generates heat which melts the layer of epoxy resin. Hence SMA wires can't be positioned at the top most layers of the fiber since it damages the smart structure.

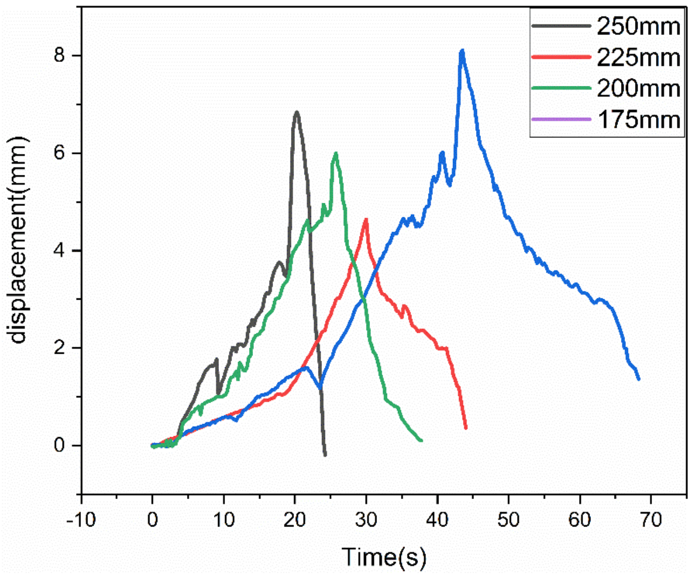

Figure 3.8 Thermo-mechanical actuation of the smart structure by varying its length

Further increase in the actuation range with optimized V_f and strain level, length of the smart structure is one of the processing parameters which optimizes the actuation rate. To optimize the range of actuation, smart structure with four different samples of length 250mm, 225mm, 200mm, and 175mm are fabricated

It is clear that smart structure length of 250mm shows a deflection of 6.98mm in 19s and subsequently come back to the initial state at 24.2s without any induced deformation. The vertical linearity of the cooling trend shows the material doesn't lose its elastic rigidity which implies that the temperature rise is less than Tg of the GFRP

Smart structure of 225mm and 200mm show comparatively low deflection value 5.97mm and 4.24mm in 27.2s and 29.4s respectively. Although the rate of deflection depends on many factors, the total length of SMA getting strained is one of the most important factor. As the length of the specimen increases, the length of SMA strained also increases. While cooling, these specimen shows a shift in the slope of the curves compared to 250mm sample, which implies that there is a loss in the elastic rigidity of the material and temperature rises beyond glass transition temperature.

Although 175mm smart structure shows the higher value of deflection 8.17mm compared to the former ones it took 46.2s to actuate. As time increases the temperature of the composite specimen also increases hence the material transforms from elastic to visco-elastic phase. From the cooling curve, it is evident that the material loses its elastic rigidity and it shows a permanent deformation of 1.24mm after its cooled.

From the above results, it has been concluded that a smart structure of length 250mm shows the reliable thermo-mechanical actuation compared to the other specimens. Hence, the length of smart structure to analyze the thermo-mechanical actuation was optimized to 250mm.

From the above results of thermo-mechanical actuation, the processing parameters are concluded and are listed in the following table

Table 3-1 Optimized processing parameters of SMA smart structure

S.No	Processing parameter	Optimized to
1	The material used for fabrication	SMA-NiTi Reinforcement-Unidirectional Glass fiber
2	SMA volume Fraction	6%
3	SMA initially strained	5%
4	Length of Smart structure	250mm

Hence, thereby I conclude the processing parameters for thermo-mechanical actuation of the smart structure. These processing parameters are remained unchanged to analyze the material properties of the smart structure.

Chapter 4 Crystallization effect on the actuation of the smart structure

4.1 Smart structure characterized through XRD

Smart structure fabricated by NiTi SMA and GFRP actuates only for a limited number of cycles. Although NiTi SMA wires actuate for a million cycles, yet the smart structure fabricated through it runs for a limited number of cycles. GFRP is a glass fiber reinforced polymer, which is generally amorphous in structure. In order to analyze the premature failure of the smart structure, material properties of GFRP were analyzed.

To analyze the primary cause for the failure of the smart structure, a sample size of 5mm length and 0.5mm was cut from the smart structure at different locations, and it was characterized under x-ray diffraction (XRD), scanning electron microscope (SEM) and differential scanning calorimeter (DSC). Different locations on the smart structure starting from the layer of GFRP next to SMA and GFRP laying in the mid zone between SMA wire are characterized under XRD. Rigaku smart lab, automated x-ray diffractometer was used for XRD characterization. All the samples are analyzed for 10^{o} to 80^{o} of two theta with a Cu target

XRD characterization at different locations on the smart structure can be seen in figure 14. It is clearly evident that GFRP next to SMA was completely crystalized. As we move towards the mid region the amount of crystallization of GFRP was gradual decreases and at the mid region, the structure was completely amorphous.

Thermo-mechanical actuation is a continuous cycle of heating and cooling in a limited time span. GFRP next to SMA are strongly subjected to this thermal gradient and it causes a change in the crystal structure of GFRP. As the distance from the SMA increases gradually the heat flux variation and the thermal gradient will be minimum which avoids the crystallization of the polymer.

The smart structure was actuated because of the strain induced in the structure in each and every cycle. As we mentioned earlier, GFRP near to SMA gets crystallized, the elastic rigidity of the GFRP structure was lost and the material act as a brittle polymer. Once GFRP becomes brittle polymer it no longer holds the SMA and it cannot induce the strain in the next cycle. Hence the structure no more actuates.

To analyze the crystallization of GFRP further, the specimens are characterized with DSC and their glass transition temperature and its shift has been clearly observed.

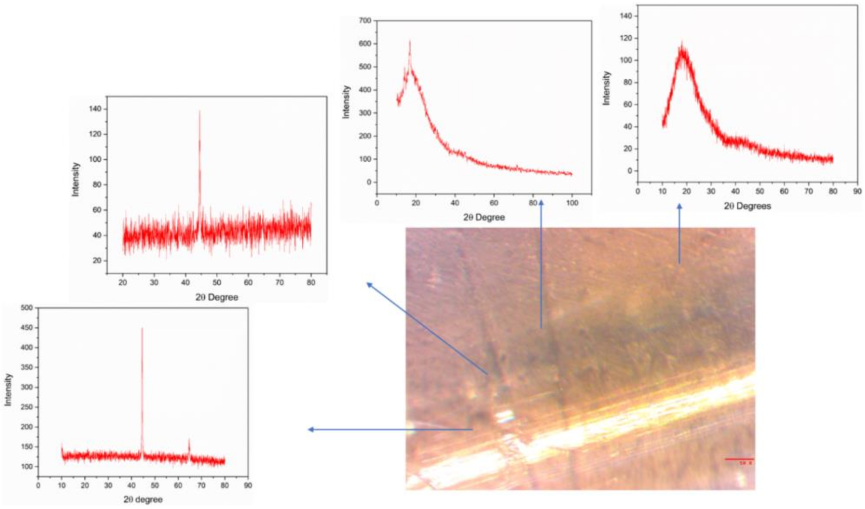

Figure 4.1 Crystallization effect at various positions on the smart structure

4.2 Evaluation of thermal properties of the smart structure using Differential Scanning Calorimeter.

Thermo-mechanical actuation of the smart structure induces a lot of change in the material properties of the smart structure. As mentioned above thermo-mechanical actuation of smart structure transforms the amorphous phase of GFRP into a crystalline phase. In order to analyze it further a 10gms sample of GFRP with SMA before and after actuation was analyzed.

Glass transition temperature (T_g) is the temperature where the material transforms form glass phase (hard and rigid) to a rubbery phase (soft and flexible). Glass transition temperature is one of the most important parameters of amorphous polymers. The temperature of an amorphous material reaches above T_g the material behaves as rubbery or viscous fluid depends on its molecular weight whereas below T_g it acts a glass (necessary structural rigidity will be provided by side chains) depending upon the complexity of the structure.

Glass transition temperature of the smart composite structure was determined experimentally. Experiments were performed by following ASTM F2004 standard, and the variation in T_g was studied at a heating/cooling rate of 10^o /min. The smart structural sample was exposed to a continuous set of heating and cooling cycles which is also a sort of thermo-mechanical loading.

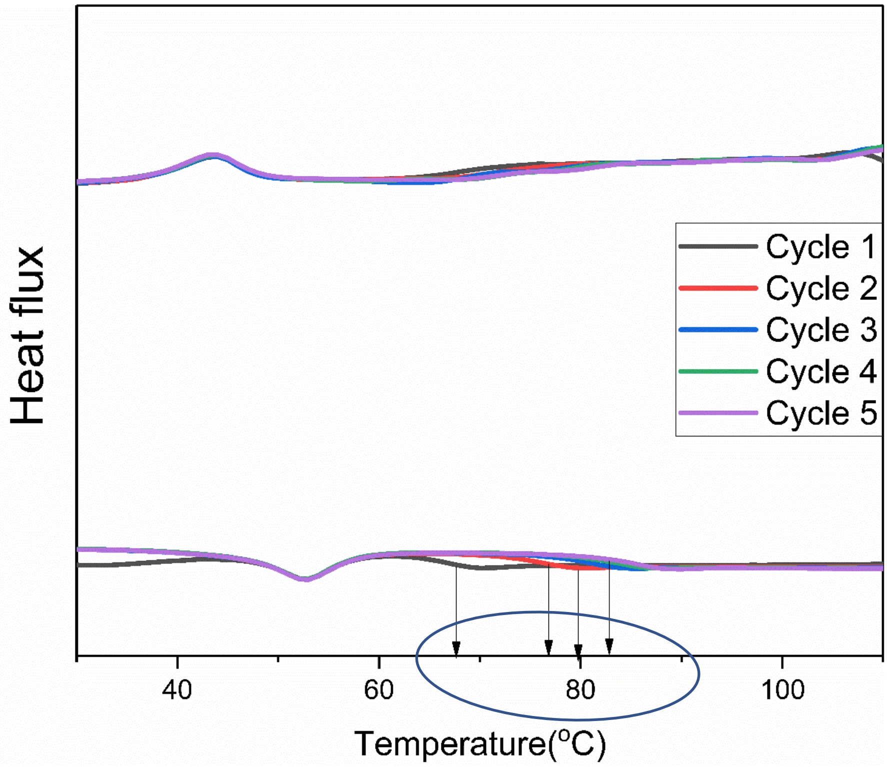

Figure 4.2 Heat flux curves of the smart composite structure before actuation

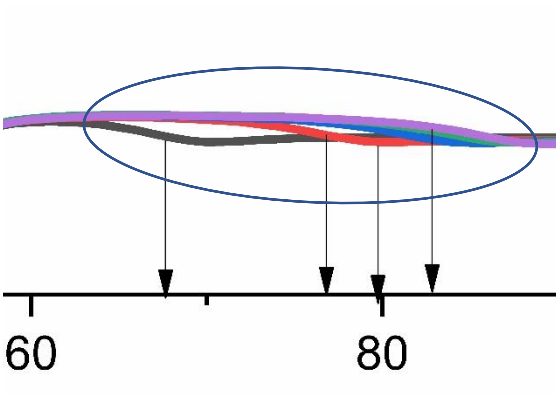

Figure 4.3 T_g of the unactuated smart structure focusing on the glass transition region

Figure 4.2, demonstrates the heat flux curves of an unactuated smart structure. Since the smart structure involves both SMA and GFRP, hence peaks appeared in the region of 40° to 60° is because of phase transformation of NiTi from martensite to austenite in heating cycle and austenite to martensite in cooling cycle. From the figure, it is clearly evident that for each and every heating/cooling cycle, there is a shift in T_g of the smart structure. As the number of cycles increases, T_g also increases but the magnitude of the shift is decreasing for each cycle and it can be seen in table 4.1. T_g of the smart structure for cycle 4 and cycle 5 doesn't show much variation as it remains almost constant. Each and every cycle of heating and cooling induces a material change in the GFRP which causes a change in the glass transition temperature.

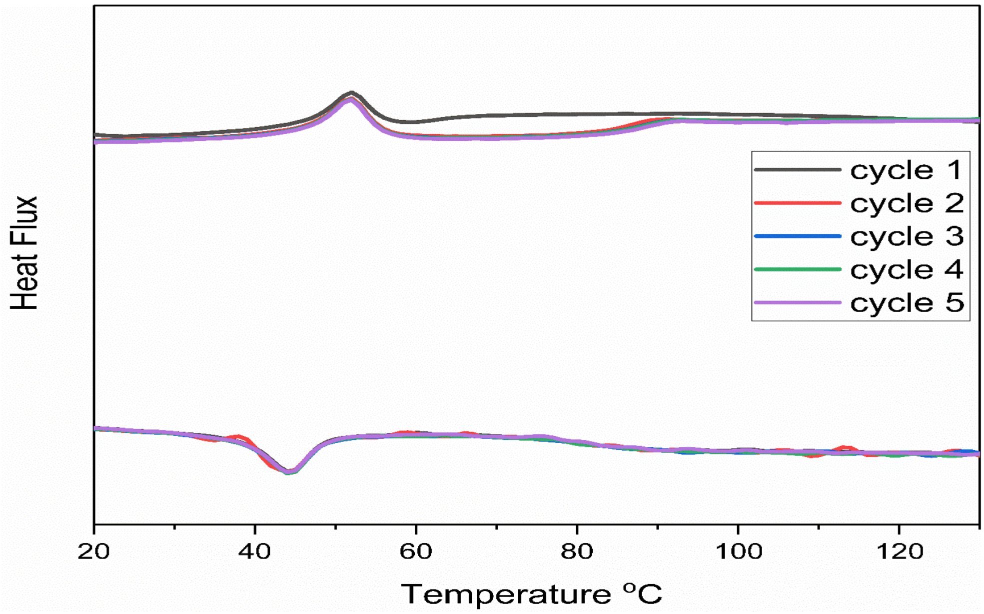

Figure 4.4 Heat flux curves of the smart composite structure after actuation

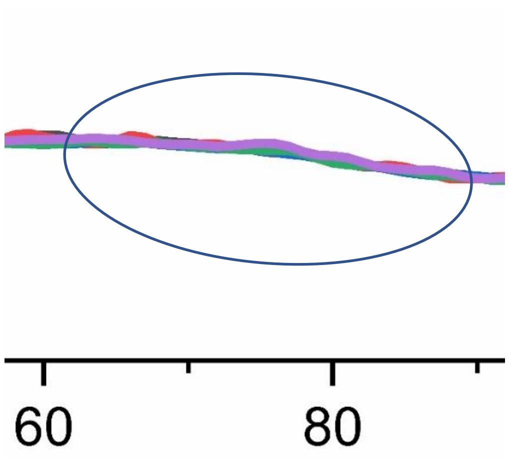

Figure 4.5 Smart structure after actuation focused at their Tg location

Above conclusion from section 4.1 that the GFRP near to SMA transforms from amorphous phase to crystalline phase needed to be justified with DSC analysis. To analyze it further now an actuated smart structure sample was analyzed with DSC for 5 sets of cycles

An actuate Smart structure sample of 10gms was analyzed with 10^{o} C/min of heating and cooling cycle. From figure 4.4, it is clearly evident that there is no change in the SMA phase transformation. Both austenitic and martensitic phase transformations are appearing at the same location. But there is no significant glass transition region appeared in the actuated smart structure in the region of 60^{o} C to 90^{o} C.

Table 4-1 Variation in T_g of SMA composite before and after actuation

S.No	Cycle	T_g (^{o} C)	Variation from the previous cycle
1	Cycle 1	68	-----------
2	Cycle 2	78	10
3	Cycle 3	80	2
4	Cycle 4	82	2
5	Cycle 5	82	0

Glass transition region appears only for amorphous materials. There won't be any glass transition region in the crystalline materials.

Since smart structure after actuated turns in to a crystalline solid, there won't be any glass transition region in the structure. Moreover, an unactuated sample of the smart structure after a certain number of cycles shows a constant glass transition region. Therefore, it can be concluded that thermo-mechanical actuation of the smart structure induces a transformation of GFRP material from amorphous to a crystalline structure.

4.3 SEM analysis on the smart structure

Thermo-mechanical actuation of smart structure induces a lot of changes in the micro structure of the material. As mentioned above the material transforms from amorphous to crystalline, still there are a lot of changes may induce in the material for the failure of the smart structure. In order to analyze further, especially the material properties, SEM is one of the best ways to determine it.

Scanning electron microscopy is one of the electron microscopies which is used to generate the image of the sample by scanning the topology of the surface with the help of an electron beam. Secondary electrons emitted from the specimen are detected by a florescent detector. Light emitted by the florescent detector is converted in to electrons. Later these electrons are amplified as an electrical signal and transferred to a display unit.

Zeiss sigma FE-SEM was used for analyzing the topology of the smart structure. Since, material properties changes after actuation, so a topological image of the smart structure before and after actuation has been analyzed.

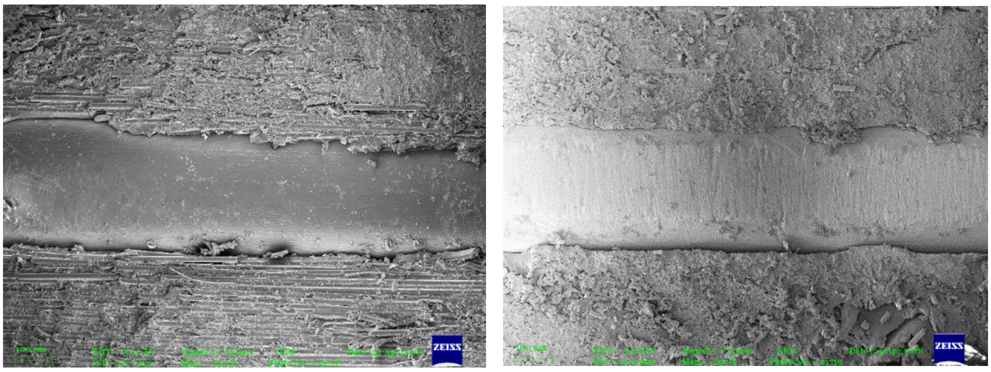

Before actuation After actuation

Figure 4.6 Surface morphology of the epoxy resin in the smart structure

Thermo-mechanical actuation of the smart structure via joule heating induces heat flow into the GFRP of the smart structure. Heat generated in turn degrades the smart structure. Figure 4.6 shown here was the top sectional view of the smart structure at the SMA and GFRP interface. It is clearly evident that at the smart structure, the GFRP lost its structural integrity and it is completely degraded.

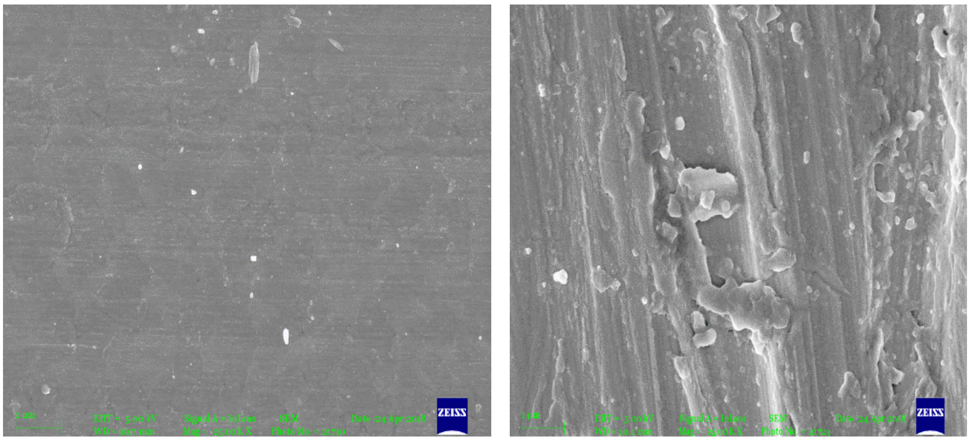

Before actuation After actuation

Figure 4.7 Flow of the epoxy resin

To analyze the structure further, at 1 μm magnification range the epoxy resin can be clearly visualized. Heat flow in the smart structure causes degradation at the SMA-GFRP interface, but at the other regions, there will be a flow of epoxy resin. The flow will be directed in direction of the thermal gradient. It can be clearly seen from figure 4.7, the plain morphology of the epoxy resin before actuation and a flow pattern after actuation.

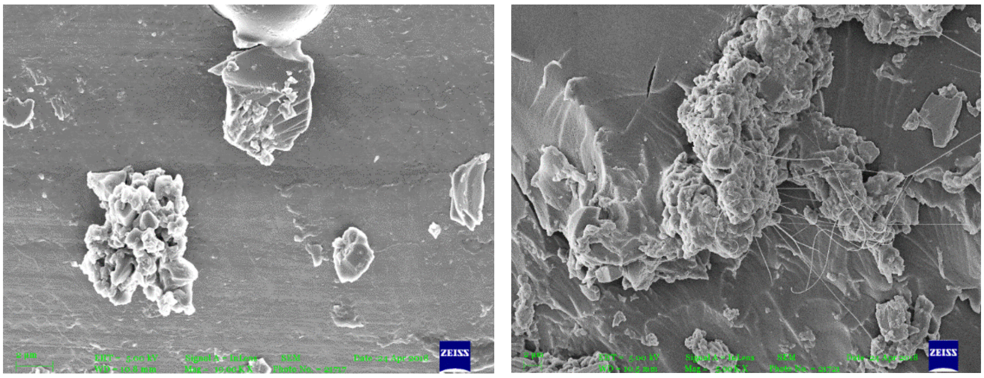

Before actuation After actuation

Figure 4.8 Agglomeration of epoxy resin

When the smart structure was set for curing, at certain regions there will be an agglomeration in the epoxy resin due to enthalpy relaxation in the smart structure under curing. Due to thermo-mechanical actuation of the smart structure, there will be an inducement of thermal energy. Actuation of the smart structure is a process of consecutive heating and cooling cycles for a short interval of time. Re-curing of the epoxy resins after thermo-mechanical actuation actually agglomeration or combining of the excess amount of epoxy at a particular location. Agglomeration of the epoxy resin can be clearly seen in figure 4.8.

Chapter 5 Variation in the surface temperature and stress distribution on the smart structure due to air flow

Thermo-mechanical actuation of the smart structure induces stress and temperature into the structure, which is inter-related with the material properties. Experimentally determining the stress and temperature are a very tedious process and time consuming. Since all the thermo-mechanical experiments are evaluated under static atmosphere conditions, it is necessary to evaluate the behavior of smart structure under dynamic conditions.

5.1 Evaluation of homogenized properties for GFRP

Smart structure fabricated by using vacuum moulding process will have maximum of 40% volume fraction. The ratio between the volume of fiber and volume of epoxy used in a GFRP defines its volume fraction. GFRP fabricated by VARTM method are tested under the universal testing machine to determine its modulus and strength. On basis of its modulus value, the V_f of the GFRP fabricated was determined. V_f determined, used for the determination of the homogenized properties of GFRP. Homogenized properties determined are used in design of smart structural model and then surface temperature and stress are determined due to thermo-mechanical actuation.

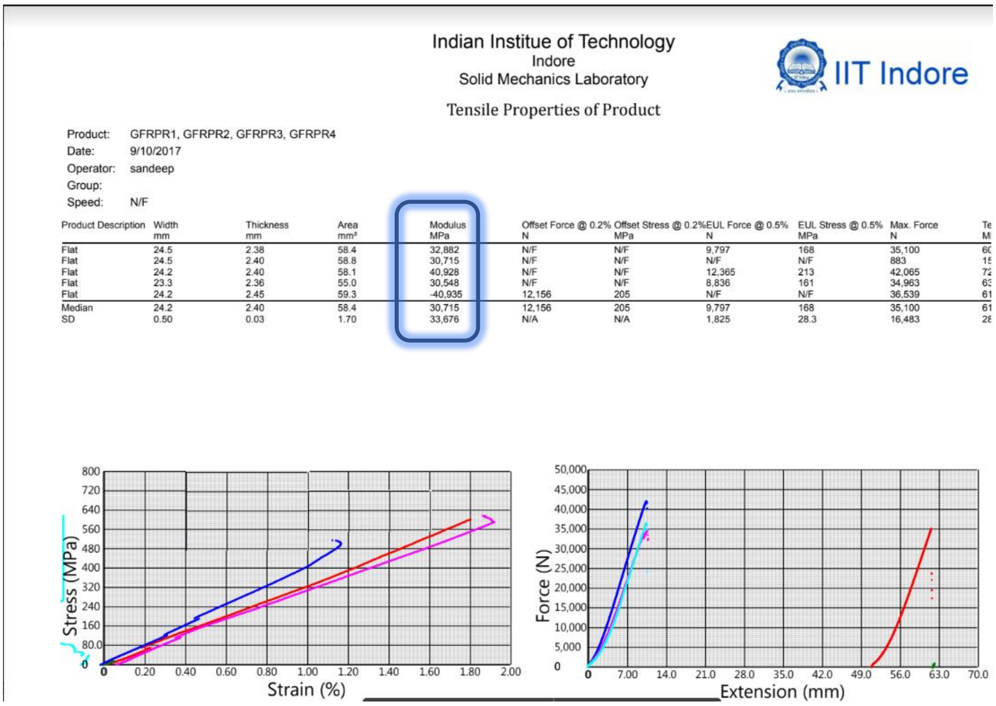
Indian Institue of Technology
Indore
Solid Mechanics Laboratory
IIT Indore

Tensile Properties of Product

Product: GFRPR1, GFRPR2, GFRPR3, GFRPR4
Date: 9/10/2017
Operator: sandeep
Group:
Speed: N/F

Product Description	Width mm	Thickness mm	Area mm²	Modulus MPa	Offset Force @ 0.2% N	Offset Stress @ 0.2% MPa	EUL Force @ 0.5% N	EUL Stress @ 0.5% MPa	Max. Force N	Te M
Flat	24.5	2.38	58.4	32,882	N/F	N/F	9,797	168	35,100	60
Flat	24.5	2.40	58.8	30,715	N/F	N/F	N/F	N/F	883	15
Flat	24.2	2.40	58.1	40,928	N/F	N/F	12,365	213	42,065	72
Flat	23.3	2.36	55.0	30,548	N/F	N/F	8,836	161	34,963	63
Flat	24.2	2.45	59.3	-40,935	12,156	205	N/F	N/F	36,539	61
Median	24.2	2.40	58.4	30,715	12,156	205	9,797	168	35,100	61
SD	0.50	0.03	1.70	33,676	N/A	N/A	1,825	28.3	16,483	28

Figure 5.1 Experimentally determining the modulus of GFRP using UTM

Modulus of GFRP are determined for 4 different samples by using UTM. It was concluded that GFRP with a modulus of 30.715 GPa was fabricated. Modulus obtained from the fabricated samples indicated that the GFRP samples are having 40% of volume fraction.

Fibre type	AS4	T300	E-glass 21xK43 Gevetex	Silenka E-Glass 1200tex
Longitudinal modulus, E_{f1} (GPa)	225	230	80	74
Transverse modulus, E_{f2} (GPa)	15	15	80	74
In-plane shear modulus, G_{f12} (GPa)	15	15	33·33	30·8
Major Poisson's ratio, ν_{f12}	0·2	0·2	0·2	0·2
Transverse shear modulus, G_{f23}	7	7	33·33	30·8
Longitudinal tensile strength, X_{fT} (MPa)	3350	2500	2150	2150
Longitudinal compressive strength, X_{fc} (MPa)	2500	2000	1450	1450
Longitudinal tensile failure strain, ε_{f1T} (%)	1·488	1·086	2·687	2·905
Longitudinal compressive failure strain, ε_{f1C} (%)	1·111	0·869	1·813	1·959
Longitudinal thermal coefficient, α_{f1} (10^{-6}/°C)	−0·5	−0·7	4·9	4·9
Transverse thermal coefficient, α_{f2} (10^{-6}/°C)	15	12	4·9	4·9

Figure 5.5.2 Mechanical properties of glass fiber

Matrix type	3501-6 epoxy	BSL914C epoxy	LY556/HT907/ DY063 epoxy	MY750/HY917/ DY063 epoxy
Manufacturer	Hercules	DFVLR	Ciba Geigy	Ciba Geigy
Modulus, E_m (Gpa)	4·2	4·0	3.35	3.35
Shear modulus, G_m (Gpa)	1·567	1·481	1·24	1·24
Poisson's ratio, ν_m	0·34	0·35	0.35	0.35
Tensile strength, Y_{mT} (MPa)	69	75	80	80
Compressive strength, Y_{mC} (MPa)	250	150	120	120
Shear strength, S_m (MPa)	50	70	—	—
Tensile failure strain, ε_{mT} (%)	1·7	4	5	5
Thermal coefficient, α_m (10^{-6}/°C)	45	55	58	58

Figure 5.5.3 Mechanical properties of the Epoxy resin

To obtain the homogenized GFRP material properties like strength and modulus of the manufactured composite specimens the individual material properties of the glass fiber and Epoxy resin are to be known initially. P. D. Soden et.al [20] calculated the mechanical properties of various glass fiber and the epoxy resin. Since E-glass with 1200 tex and HY917 are used in fabrication, hence their properties were taken in determination of homogenized properties of smart structure. Homogenized mechanical properties of the GFRP are calculated for 40% of volume fraction. Chamis [21] et.al' micro-mechanical homogenization formulae are taken in to consideration for calculating the homogenized properties. Following are the list of formulae for evaluating the homogenized properties GFRP with a significant volume fraction.

Table 5-1 Formulae for determining homogenized properties of GFRP

Properties	**Formulae**
Longitudinal Modulus:	$E_{11} = V_f E_{f11} + V_m E_m$
Transverse Modulus:	$E_{22} = E_{33} = \frac{E_m}{1-\sqrt{V_f\left(1-\frac{E_m}{E_{f22}}\right)}}$
Shear Moduli:	$G_{12} = G_{13} = \frac{G_m}{1-\sqrt{V_f\left(1-\frac{G_m}{G_{f12}}\right)}}$
Shear Modulus:	$G_{23} = \frac{G_m}{1-\sqrt{V_f\left(1-\frac{G_m}{G_{f23}}\right)}}$
Poisson's ratio:	$\nu_{12} = \nu_{13} = V_f \nu_{f12} + V_m \nu_m$
Poisson's ratio:	$\nu_{23} = \frac{E_{22}}{2G_{23}} - 1$
Longitudinal Tensile strength:	$\sigma_t = V_f \sigma_f$
Longitudinal Compressive strength:	$\sigma_c = V_f \sigma_c$
Transverse Tensile strength:	$\sigma_t^T = \left[1 - \left(\sqrt{V_f} - V_f\right)\left(1 - \frac{E_m}{E_{f_{22}}}\right)\right]\sigma_m^T$
Transverse Compressive strength:	$\sigma_c^T = \left[1 - \left(\sqrt{V_f} - V_f\right)\left(1 - \frac{E_m}{E_{f_{22}}}\right)\right]\sigma_m^c$
Shear Strength:	$\tau_s = \left[1 - \left(\sqrt{V_f} - V_f\right)\left(1 - \frac{G_m}{G_{f_{22}}}\right)\right]\tau_m^s$

Table 5-2 Homogenized values of GFRP for 40% of volume fraction

Mechanical properties	Homogenized values of GFRP
Longitudinal Modulus E_{11},GPa	31.61
Transverse Moduli E_{22}, E_{33}, GPa	8.77
Shear Moduli G_{12}, G_{13}, GPa	3.26
Shear Modulus G_{23} GPa	3.26
Poisson's ratio ν_{12}, ν_{13}	0.29
Poisson's ratio ν_{23}	0.3451
Longitudinal Tensile strength, MPa	860
Longitudinal Compressive strength, MPa	580
Transverse Tensile strength, MPa	62.2
Transverse Compressive strength, MPa	93.36
Shear Strength, MPa	54.38

5.2 Modelling of the smart structure

Smart structure model properties determined from chapter 4 are used and the structure was fabricated using SOLID WORKS design software. A smart structure designed, is of 250mm length with 6% of SMA volume fraction and strained up to 5%.

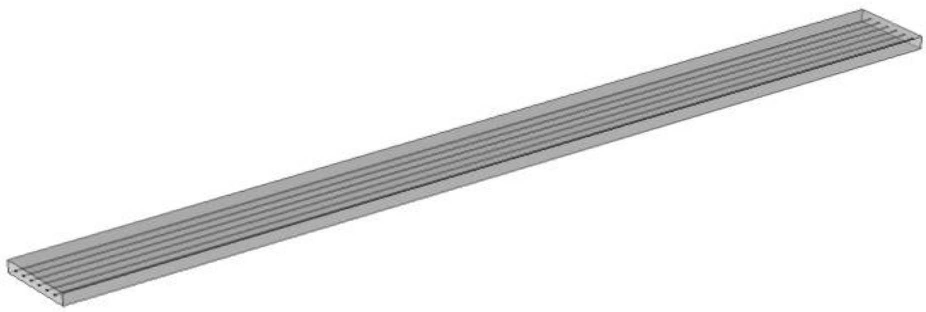

Figure 5.4 Smart structure modelled in solidwork

5.3 Boundary conditions

To analyze the impact of wind velocity on the thermal gradient of the smart structure, air with different flow velocities were considered. Flow velocities of 1, 5, 9, 13, 17 are taken into the consideration. A constant current of 10V and 2A was applied at one terminal and the other terminals are maintained at neutral. Enclosure with 300mm×200mm×150mm was created to maintain constant air flow.

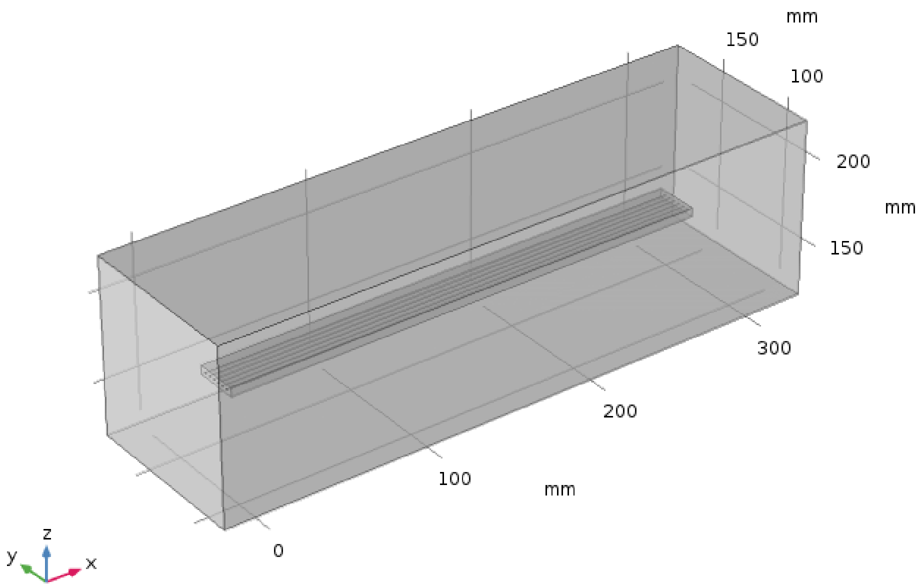

Figure 5.5 Model of the smart structure with an enclosure

5.4 Mesh considerations for the smart structure and the enclosure

Smart structure model meshed with a fine mesh whereas the enclosure meshed with coarse mesh in order to minimize the overall computation time.

Table 5-3 Properties of the Mesh

S.No	Mesh element	Value
1	Vertex elements	40
2	Edge elements	7296
3	Boundary elements	44934
4	Total no of elements	846013
5	Minimum element quality	0.1479

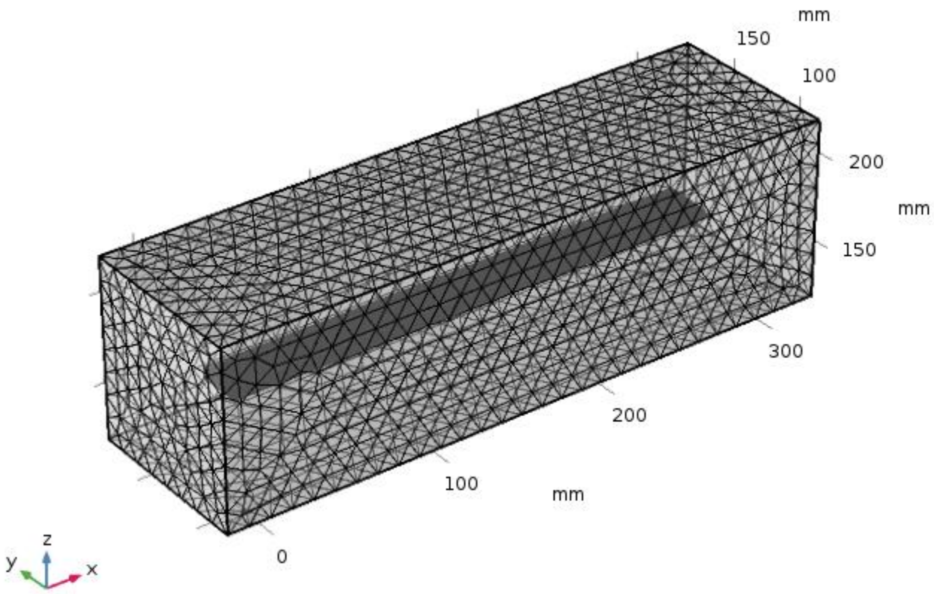

Figure 5.6 Smart structure with enclosure meshed in to elements

5.4 Variation in the thermal profile of smart structure with respect to the airflow

Thermo-mechanical actuation of the smart structure involves generation of heat from the specimen. We had discussed in chapter 4 that the thermal gradient will vary at different places on the smart structure. The primary application of the fabricated smart structure was flapper of a missile wing. Therefore, in a real application, the smart structure was subjected to the various other parameters like surface temperature, stress generation, air flow, turbulence, lift and drag parameters etc. All the above mentioned parameters are to be identified and their impact on the smart structure should be evaluated. Out of all the parameters, the effect of air velocity over the smart structure was my primary interest since the structure is flat, there won't be any lift coefficient on the missile. Currently, the parameters like temperature and stress are evaluated on the smart structure by varying the velocity of air flow. Hence a software based simulation, COMSOL was used in order to determine the characteristic performance of the smart structure with respect to these parameters.

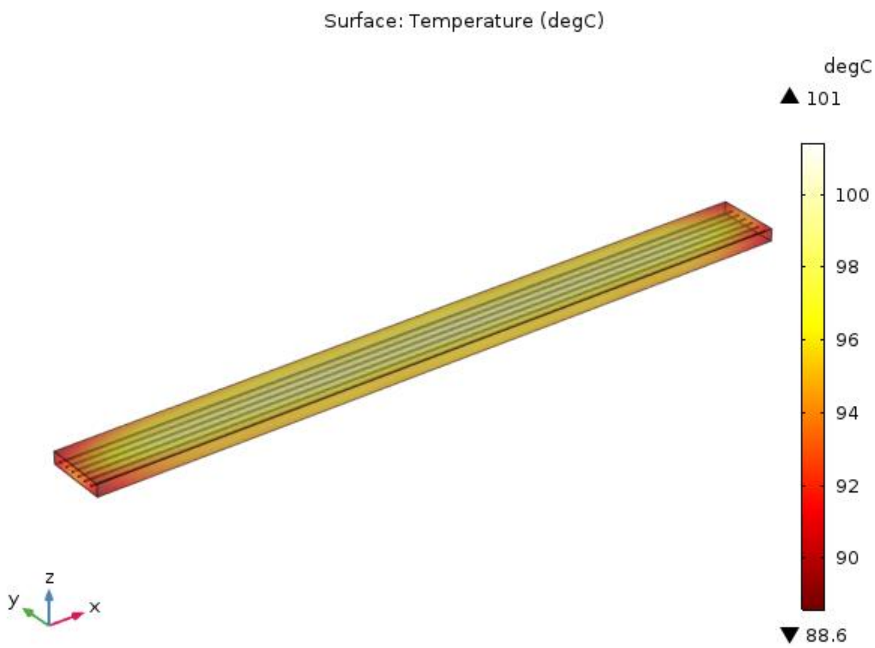

Figure 5.7 surface temperature of the smart structure with no air flow

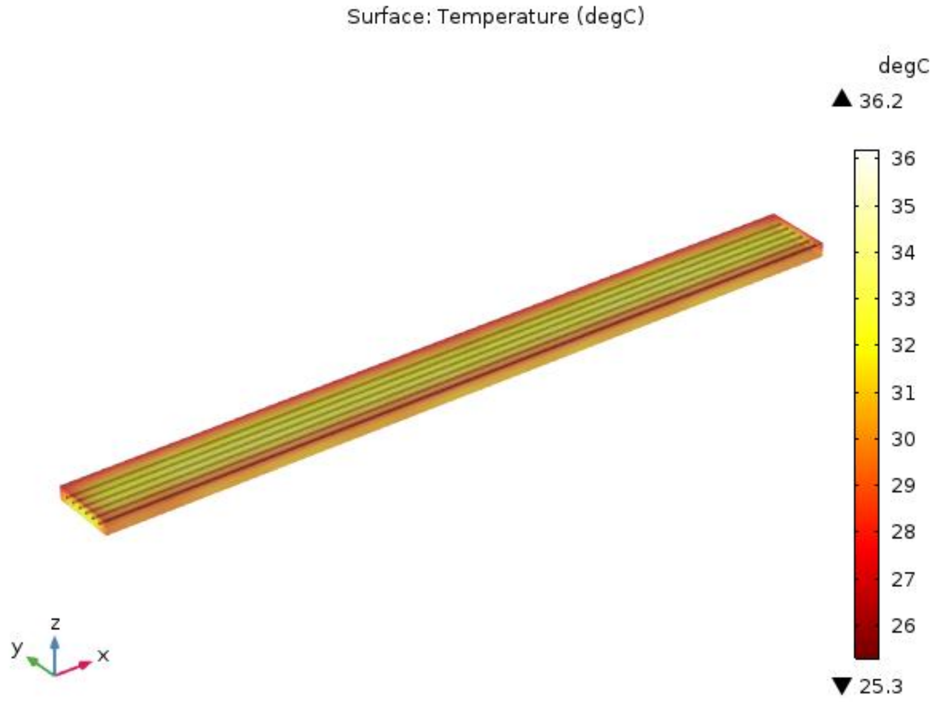

Figure 5.8 surface temperature of the smart structure with an air flow of 1 m/s

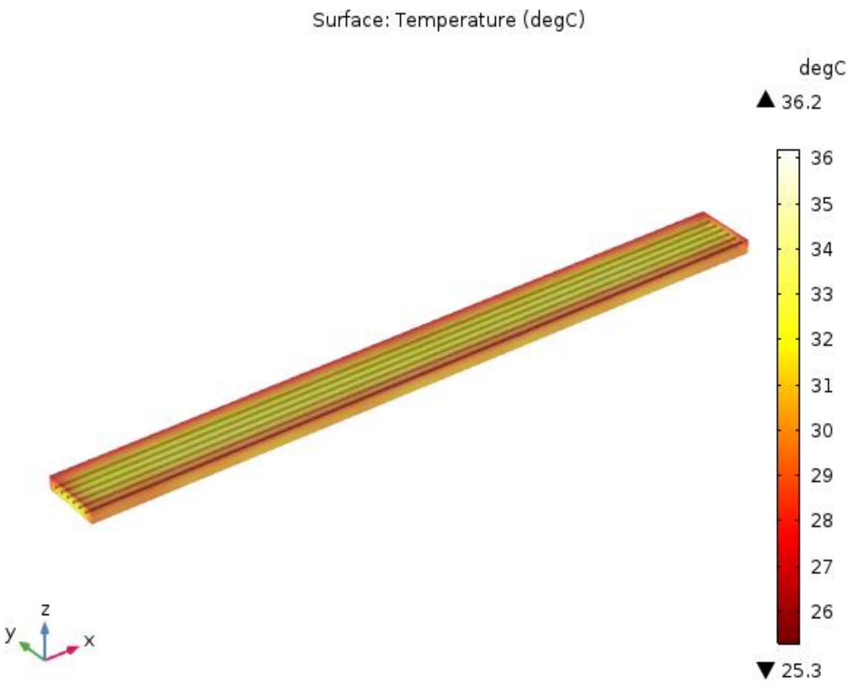

Figure 5.9 surface temperature of the smart structure with an air flow 5 m/s

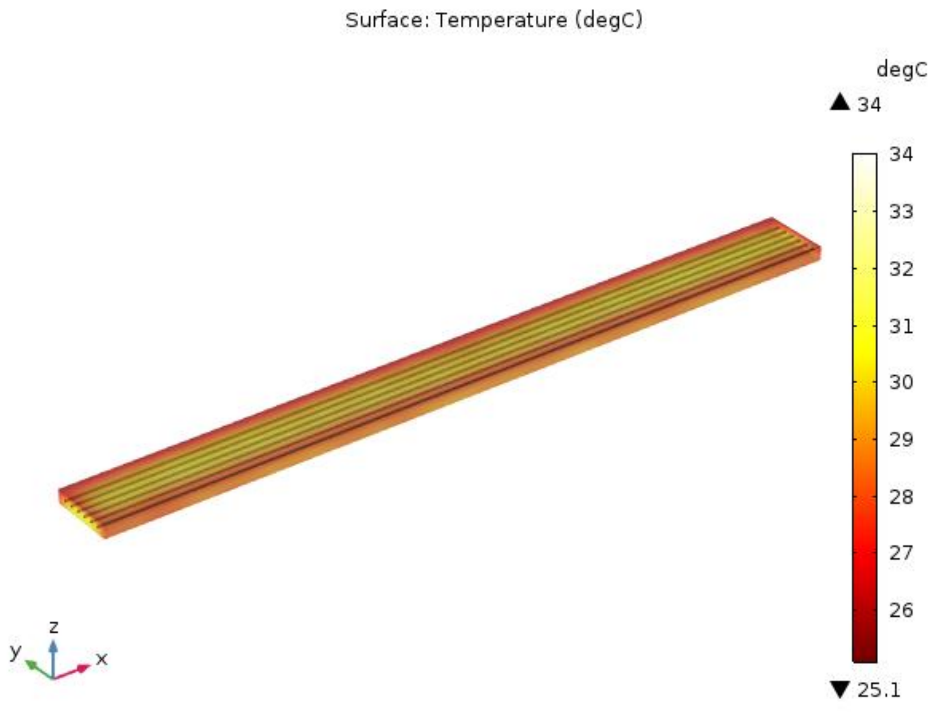

Figure 5.10 surface temperature of the smart structure with an air flow 9 m/s

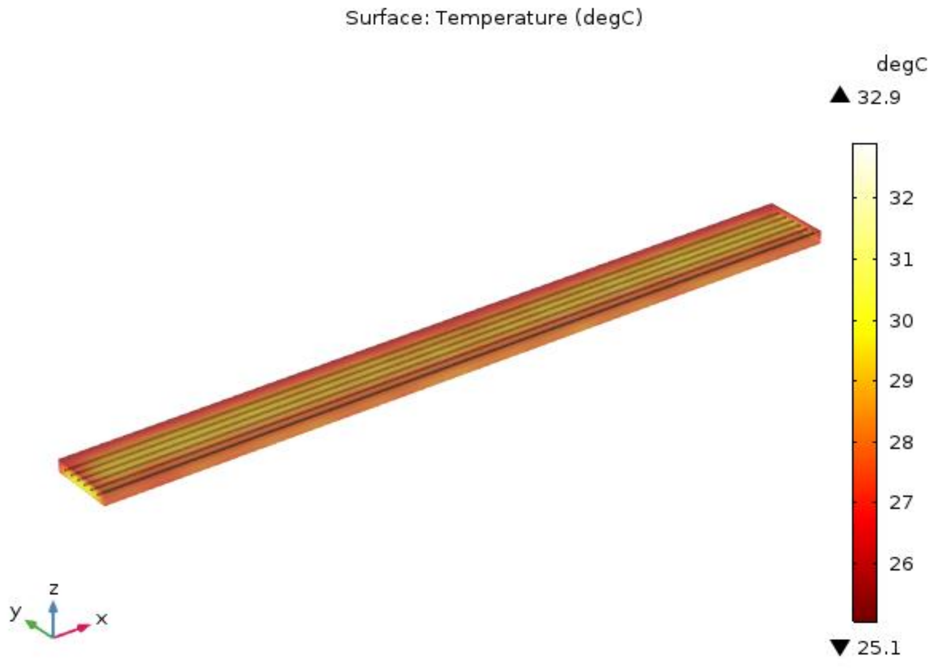

Figure 5.11 surface temperature of the smart structure with an air flow 13 m/s

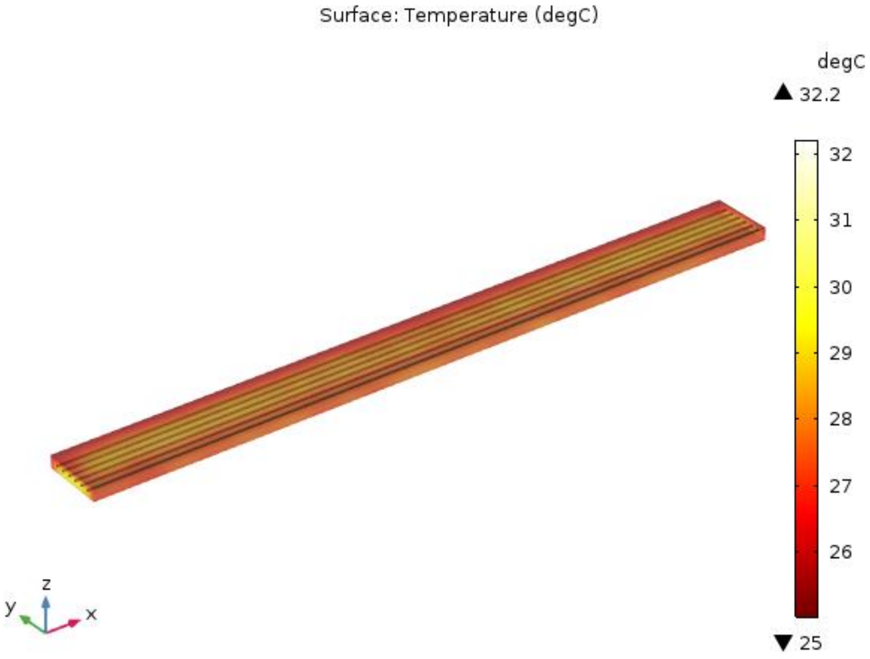

Figure 5.12 surface temperature of the smart structure with an air flow 17 m/s

It is clearly evident that when the velocity of the air was increased to 1 m/s there was a drastic decrease in the surface temperature of the smart structure. Further increase in the velocity doesn’t cause many variations in the surface temperature. Hence, minimum velocity of the wind 1 m/s is sufficiently enough to bring back the temperature of the smart structure below its glass transition temperature.

5.5 Determination of stress generated in the smart structure due to air flow

Thermo-mechanical actuation of the smart structure induces stress into the GFRP. Since GFRP being a structural member of the smart structure, it is necessary to evaluate the quantity of stress generated into it. Generally, the developed smart structure is used in aviation applications. Hence the primary mode to induce stress is due to air flow. Stress generated in the smart structure is evaluated for various velocities of air flow. The following figures represent the variation in the generation of stress on the smart structure

The primary objective of this simulation was to ensure that stress developed in the smart structure is less than the failure stress of the structure. Beginning of the chapter we calculated the homogenized properties of the GFRP. Hence the stress generated in the smart structure should be less than the homogenized stress values.

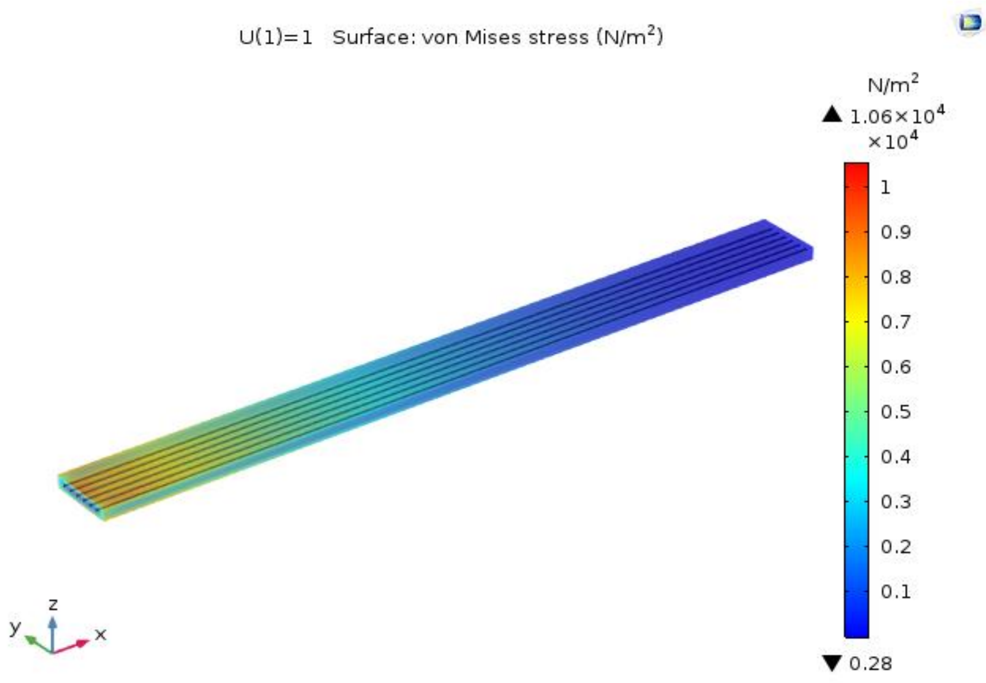

Figure 5.13 Stress generated in the smart structure with an air velocity of 1 m/s

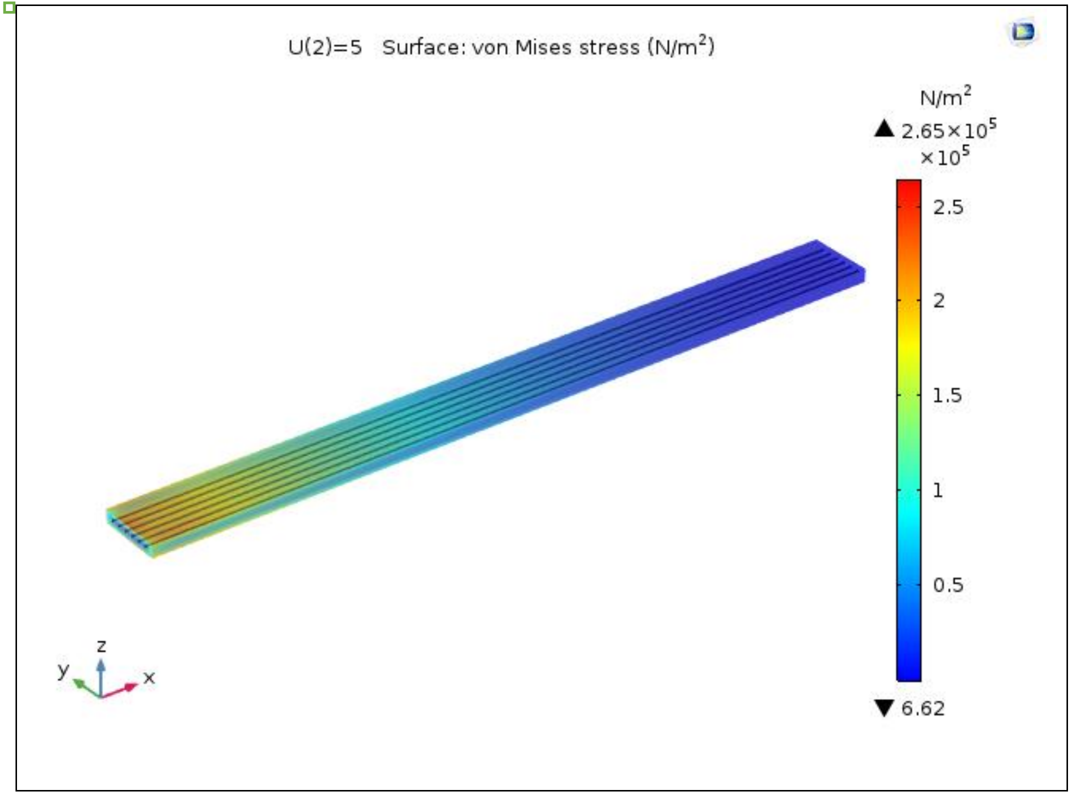

Figure 5.15 Stress generated in the smart structure with an air velocity of 5 m/s

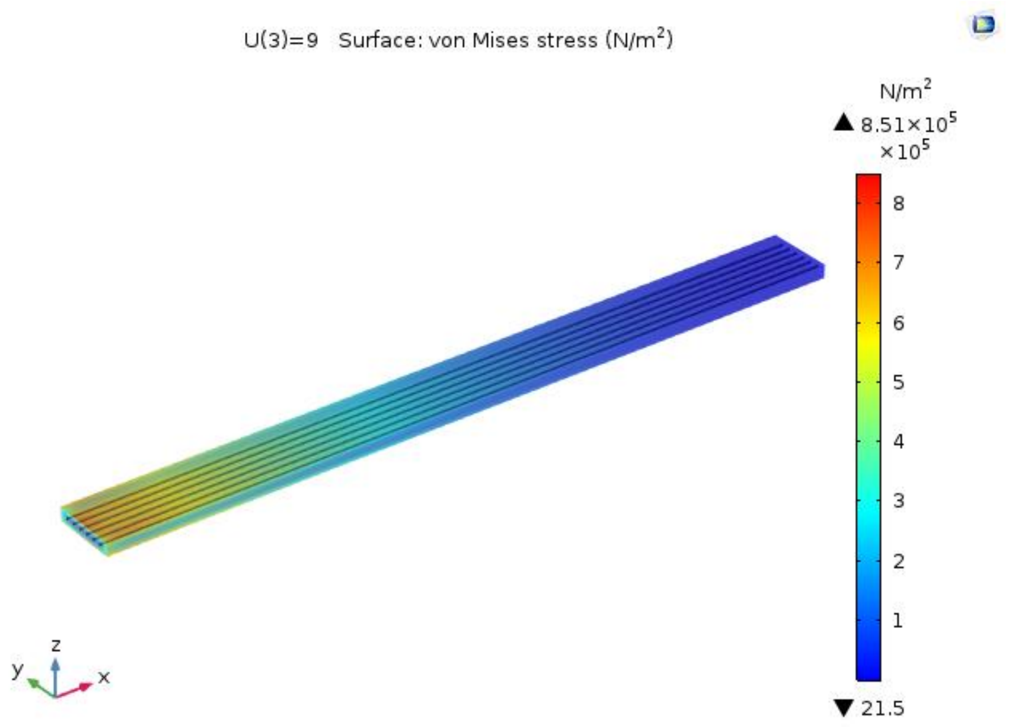

Figure 5.14 Stress generated in the smart structure with an air velocity of 9 m/s

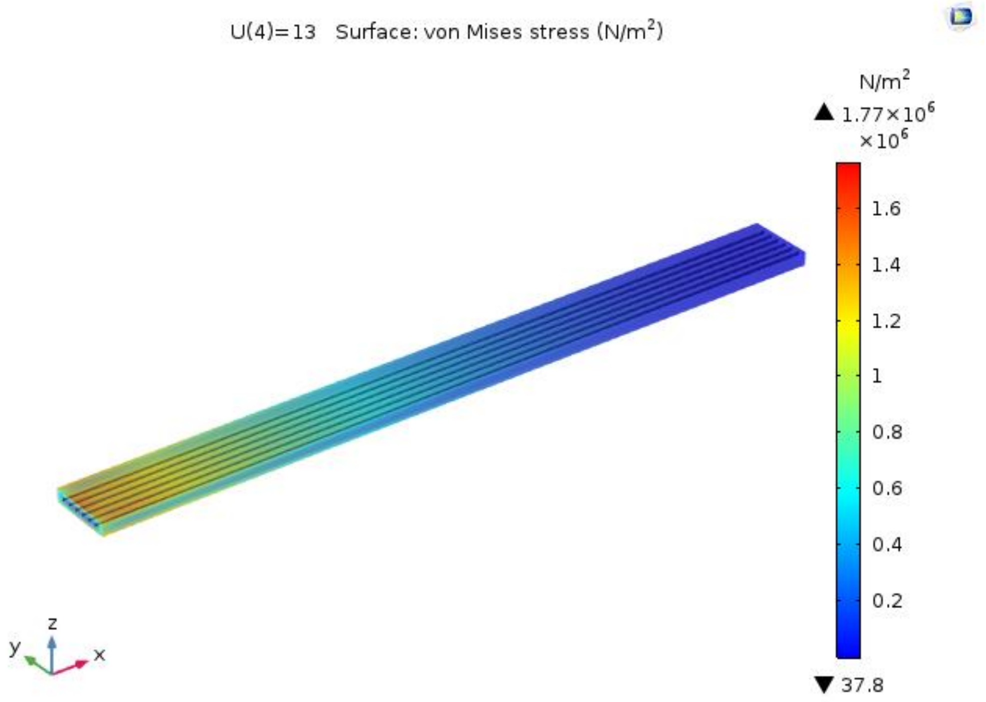

Figure 5.16 Stress generated in the smart structure with an air velocity of 13 m/s

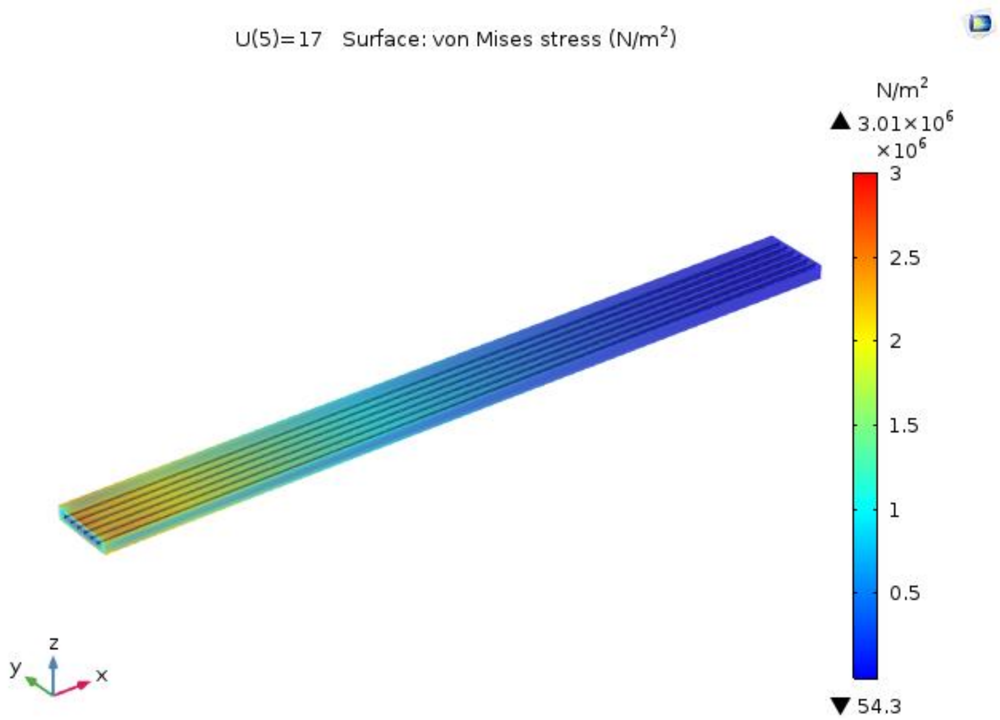

Figure 5.17 Stress generated in the smart structure with an air velocity of 17 m/s

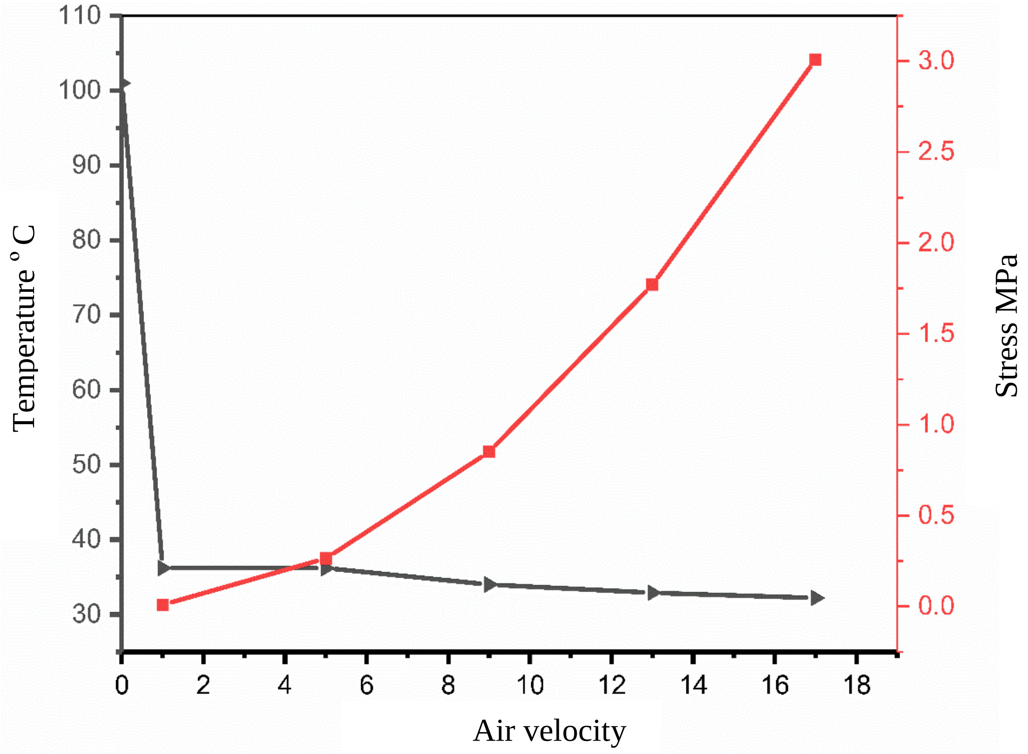

Figure 5.18 Temperature and stress distribution on the smart structure

Form figure 5.18 it is clearly evident that when the velocity of the stress developed in the smart structure was 3MPa. Since the shear stress of the current structure was very near to the developed smart structure, hence there could be a possible shear failure in the smart structure. As the flow velocity of air was increased initially there was a sudden decrease in temperature (heat flow rate is high) but thereafter it decreases gradually. Whereas the stress was increased gradually with the velocity of air flow. Hence the optimized air flow velocity for the developed structure was 14 m/s to 16 m/s with a surface temperature ranges from 33^{o} C to 32^{o} C and the stress developed ranges from 1.7 MPa to 2.8 MPa.

Chapter 6 Conclusion and Future scope

In summary, the work performed provides a systematic study in the fabrication of the smart structure using VARTM process. Processing parameters like SMA volume fraction, length of SMA strained and length of the smart structure developed was studied. Post experimental analysis was carried out to identify the causes for the failure of the smart structure. Additionally, the effect of surface temperature and the stress generated in the smart structure by varying the air flow velocity was also studied.

The major conclusions of the current work are

1. Thermo-mechanical actuation of the smart structure was optimized with 6% of SMA volume fraction, 5% of SMA strain and 250mm length of the smart structure.
2. Thermo-mechanical actuation of the smart structure via joule heating causes the crystallization of the amorphous polymer. GFRP next to SMA was crystallized and it loses its elastic rigidity after 7 cycles.
3. Glass transition temperature of the GFRP was around 62^{o}C and it was increased to 82^{o}C after 5 cycles. Heat flux graphs of actuated GFRP didn’t show any glass transition region which confirms GFRP crystalized due to thermo-mechanical actuation.
4. After actuation GFRP was subjected to degradation, there was a flow pattern on the epoxy resin region and the amalgamation of the epoxy resin was also identified.
5. It was identified the developed smart structure has 40% of volume fraction in terms of resin fibre ratio. Homogenized properties are evaluated for the 40% of volume fraction.
6. Temperature and Stress distribution on the smart structure was evaluated by using COMSOL multi-physics. Variation in surface temperature and stress distribution due to air flow velocity was also analyzed. Air flow velocity from 1 m/s to 14 m/s - 16 m/s was the maximum range where the smart structure withstands the generated stress values.

The work presented in this dissertation have highlighted the optimized processing parameters for the thermo-mechanical actuation and its effect on the material properties. Active control on thermo-mechanical actuation of smart structure requires further effort. Optimizing the process parameters of the smart structure under active control will further increase the life of the smart structure.

Crystallization of GFRP was one of the major reason for the limited number of actuation cycles. Training of SMA rather than straining may be an optimal solution for the increment of the life cycle.

References

[1] S. Barbarino, E.L. Saavedra Flores, R.M. Ajaj, I. Dayyani, M.I. Friswell, A review on shape memory alloys with applications to morphing aircraft, Smart Mater. Struct. 23 (2014). doi:10.1088/0964-1726/23/6/063001.

[2] P. Popov, D.C. Lagoudas, Shape Memory Alloys, 2010. doi:10.1007/978-0-387-47685-8.

[3] M. Moallem, Deflection control of a flexible beam using, 12 (2003) 1023–1027.

[4] A.J. Zak, M.P. Cartmell, W.M. Ostachowicz, M. Wiercigroch, One-dimensional shape memory alloy models for use with reinforced composite structures, Smart Mater. Struct. 12 (2003) 338–346. doi:10.1088/0964-1726/12/3/304.

[5] S. Karmakar, N. Kalita, A. Banerjee, Optimum placement of shape memory alloy wire actuator, Proc. Inst. Mech. Eng. Part C J. Mech. Eng. Sci. 0 (2016) 0954406216665134. doi:10.1177/0954406216665134.

[6] G. Song, B. Kelly, B.N. Agrawal, Active position control of a shape memory alloy wire actuated composite beam, Smart Mater. Struct. 9 (2000) 711–716. doi:10.1088/0964-1726/9/5/316.

[7] A. Fortini, M. Merlin, C. Soffritti, A. Suman, G.L. Garagnani, Study of an active deformable structure with embedded NiTi shape memory alloy strips, Metall. Ital. 107 (2015) 23–30.

[8] M. Merlin, M. Scoponi, C. Soffritti, A. Fortini, R. Rizzoni, G.L. Garagnani, On the improved adhesion of NiTi wires embedded in polyester and vinylester resins, Frat. Ed Integrita Strutt. 31 (2015) 127–137. doi:10.3221/IGF-ESIS.31.10.

[9] A. Fortini, A. Suman, M. Merlin, G.L. Garagnani, Morphing blades with embedded SMA strips: An experimental investigation, Mater. Des. 85 (2015) 785–795. doi:10.1016/j.matdes.2015.07.175.

[10] A. Suman, A. Fortini, N. Aldi, M. Pinelli, M. Merlin, Using shape

memory alloys for improving automotive fan blade performance: experimental and computational fluid dynamics analysis, Proc. Inst. Mech. Eng. Part A J. Power Energy. 229 (2015) 477–486. doi:10.1177/0957650915589674.

[11] A. Suman, A. Fortini, M. Merlin, A Shape Memory Alloy-based morphing axial fan blade: Functional characterization and perspectives, Energy Procedia. 82 (2015) 273–279. doi:10.1016/j.egypro.2015.12.033.

[12] A. Suman, A. Fortini, N. Aldi, M. Merlin, M. Pinelli, A Shape Memory Alloy-Based Morphing Axial Fan Blade—Part II: Blade Shape and Computational Fluid Dynamics Analyses, J. Eng. Gas Turbines Power. 138 (2015) 062604. doi:10.1115/1.4031760.

[13] A. Fortini, M. Merlin, R. Rizzoni, S. Marfia, TWSME of a NiTi strip in free bending conditions: Experimental and theoretical approach, Frat. Ed Integrita Strutt. 8 (2014) 74–84. doi:10.3221/IGF-ESIS.29.08.

[14] H. Rodrigue, W. Wang, B. Bhandari, M.W. Han, S.H. Ahn, Cross-shaped twisting structure using SMA-based smart soft composite, Int. J. Precis. Eng. Manuf. - Green Technol. 1 (2014) 153–156. doi:10.1007/s40684-014-0020-5.

[15] R. Wu, M.W. Han, G.Y. Lee, S.H. Ahn, Woven type smart soft composite beam with in-plane shape retention, Smart Mater. Struct. 22 (2013). doi:10.1088/0964-1726/22/12/125007.

[16] H.J. Kim, S.H. Song, S.H. Ahn, A turtle-like swimming robot using a smart soft composite (SSC) structure, Smart Mater. Struct. 22 (2013). doi:10.1088/0964-1726/22/1/014007.

[17] W. Wang, J.Y. Lee, H. Rodrigue, S.H. Song, W.S. Chu, S.H. Ahn, Locomotion of inchworm-inspired robot made of smart soft composite (SSC), Bioinspiration and Biomimetics. 9 (2014). doi:10.1088/1748-3182/9/4/046006.

[18] W. Huang, On the selection of shape memory alloys for actuators, Mater. Des. 23 (2002) 11–19. doi:10.1016/S0261-3069(01)00039-5.

[19] S. Ekşi, K. Genel, Comparison of mechanical properties of unidirectional and woven carbon, glass and aramid fiber reinforced epoxy composites, Acta Phys. Pol. A. 132 (2017) 879–882. doi:10.12693/APhysPolA.132.879.

[20] P.D. Soden, M.J. Hinton, A.S. Kaddour, LAMINA PROPERTIES, LAY-UP CONFIGURATIONS AND LOADING CONDITIONS FOR A RANGE OF FIBRE-REINFORCED COMPOSITE LAMINATES, 58 (1998).

[21] T. Memorandum, Mechanics of Composite Materials : Past, Present, and Future, (2018).